ELSEVIER

Coordination Chemistry Reviews 224 (2002) 87–109

COORDINATION CHEMISTRY REVIEWS

www.elsevier.com/locate/ccr

Intercalation chemistry of molybdenum disulfide

E. Benavente, M.A. Santa Ana, F. Mendizábal, G. González *

Department of Chemistry, Faculty of Sciences, Universidad de Chile, PO Box 653, Santiago de Chile, Chile and Department of Chemistry, Universidad Tecnológica Metropolitana, José Pedro Alessandri 1242, Santiago de Chile, Chile

Received 2 October 2000; accepted 30 May 2001

Contents

Abstract

Most relevant features of the fundamental and applied chemistry of MoS_2 are reviewed highlighting the importance of the layered nature of the solid on the optical and catalytic properties of the compounds. Experimental and theoretical aspects related

* Corresponding author. Tel.: +56-2-678-7255; fax: +56-2-271-3888.
E-mail address: ggonzale@abello.dic.uchile.cl (G. González).

PII: S0010-8545(01)00392-7

to the 2H-1T-MoS_2 phase change induced by the insertion of lithium are discussed. The principal systems known until this moment, specifically those based on the intercalation of molecular and polymeric organic donors, organometallic species and cations into MoS_2 as well as the methods used for their synthesis, are described. The main characteristic of the products, principally their properties as mixed conductors and the diffusion of lithium inside the interlamellar spaces are discussed.

Keywords: Intercalation chemistry; Molybdenum disulfide

1. Introduction

One important field in the chemistry of the inclusion compounds is the study of the host–guest solids arising from the intercalation of atomic or molecular species into layered matrices like graphite, many natural clays or transition metal derivatives [1,2].

In recent decades, there has been a sustained development in the intercalation chemistry of layered transition metal chalcogenides [3]. The fundamental knowledge on the nature and properties of these compounds, largely dominated by subtle host–guest interactions and chemical recognition phenomena generates much interest [3–5]. Moreover, these essentially anisotropic materials can be used as model systems for determining the influence of the dimensionality on the properties of the compounds [6,7]. The numerous technical applications of these solids have also been an important driving force behind the development of this chemistry [8–10].

Although the intercalation chemistry of transition metal sulfide was well known even in the 1970s, the development of the molybdenum disulfide chemistry is relatively recent. The characteristics of MoS_2 and the differences between its intercalation chemistry with that of other transition metals should be found in the coordination properties of molybdenum as well as of the ligand field defined in the interlaminar spaces of the compound.

In this paper, selected features of the intercalation chemistry of molybdenum disulfide will be reviewed. In the first part, the occurrence, structure and principal properties of the matrix, as well as the principal applications of MoS_2 and MoS_2-based intercalation compounds will be discussed. The second and third parts will focus on the synthesis and properties of the lithium intercalates and on the cointercalation of lithium and donor species, respectively.

2. Molybdenum disulfide

2.1. Occurrence and synthesis

Molybdenum disulfide, 'molybdenite', is the principal natural source of molybdenum. The MoS_2 concentration in the ores is generally rather low but it can be concentrated by foam flotation [11,12]. Currently, molybdenite is mainly obtained as a secondary product from the mining of copper [12,13].

Synthetically, MoS_2 is obtained by heating molybdenum dioxide, molybdenum trioxide, or ammonium molybdate under a hydrogen sulfide flow [14,15]. It is also obtained as a microcrystalline product from the elements by prolonged heating at 1100 °C [12]. From the reaction of lithium sulfide with molybdenum chloride, MoS_2 may be obtained as an amorphous material with high surface area [16]. From the reaction of molybdenum hexacarbonyl with H_2S in microwave plasma [17], or assisted by a CO_2 laser irradiation [18], nanosized MoS_2 particles may be obtained. As thin films, useful for a series of modern applications, MoS_2 can be obtained by a variety of techniques such as radio frequency sputtering [19], pulsed laser evaporation [20,21], chemical vapor transport [20–22], and metal organic vapor deposition (MOCVD) [23,24]. Recently, polycrystalline, continuous, uniform thin films of molybdenum disulfide with a band gap energy of about 1.7 eV have also been prepared by electrodeposition from an aqueous bath of molybdenum trioxide and a thiosulfate salt [25].

Molybdenum disulfide has also been obtained as a fullerene-like material, as inorganic fullerenes (IF), by a gas phase reaction from MoO_3 [26,27]. The reaction of oxide particles smaller than 0.2 μm with H_2S in a reducing atmosphere at temperatures of about 900 °C generates a closed layer of MoS_2, which isolates the nanoparticles from its surroundings and prevents the fusion into larger particles [28]. The product consists of roughly sphero-symmetric shaped IF-MoS_2 nanoparticles with diameter > 10 nm. Similar to carbon derivatives, inorganic fullerenes as the IF-MoS_2 display negative curvatures leading to nanoparticles with complicated topologies [29]. Recently, the synthesis of microscopic nanofibers and nanotubules of MoS_2 have also been reported [30]. These products are obtained by the thermal decomposition of ammonium salts of the molybdate anions $[MoS_4]^{2-}$ and $[Mo_3S_{13}]^{2-}$ within the confined voids of a porous aluminum oxide membrane used as a template.

2.2. Structure

Three polytype modifications of MoS_2 have been described until now. The 1T-MoS_2 with the molybdenum atoms coordinated octahedrically by the sulfur

atoms and one Mo atom per unit cell (CdI_2 type) [31]; the $2H_c$-MoS_2 with trigonal prismatic coordination around the molybdenum and two S–Mo–S units per elemental cell; and the 3R-MoS_2, also with trigonal prismatic coordination but with three S–Mo–S units in the *c*-axis direction [32]. 1T-MoS_2 and 3R-MoS_2 polytypes are metastable. However, H_c-MoS_2 is a stable modification at normal conditions, crystallizing in the space group $P6/mmc$ with S-positions in ($\pm 1/3$ $\pm 2/3$ $\pm 3/4-z$) (Site B) and ($\pm 2/3$ $\pm 1/3$ $\pm 5/4-z$) (Site C) and Mo in ($\pm 1/3$ $\pm 2/3$ $\pm 1/4$) (Site c) and (2/3 1/3 z''') (Site b) with $z = 0.121$ [8]. Therefore, the arrangement of the MoS_2-units in the *c* direction may be described as BcB/CbC [33]. However, there is some confusion in the literature about the nomenclature used for the MoS_2 polytypes [2,34], specifically concerning the name of the most stable phase. This phase is often referred to as the $2H_b$-MoS_2. Therefore, in this article we will refer to this phase only as 2H-MoS_2 or simply MoS_2. The main structural features of the polytypes 2H-MoS_2 and 1T-MoS_2 are illustrated in Fig. 1a.

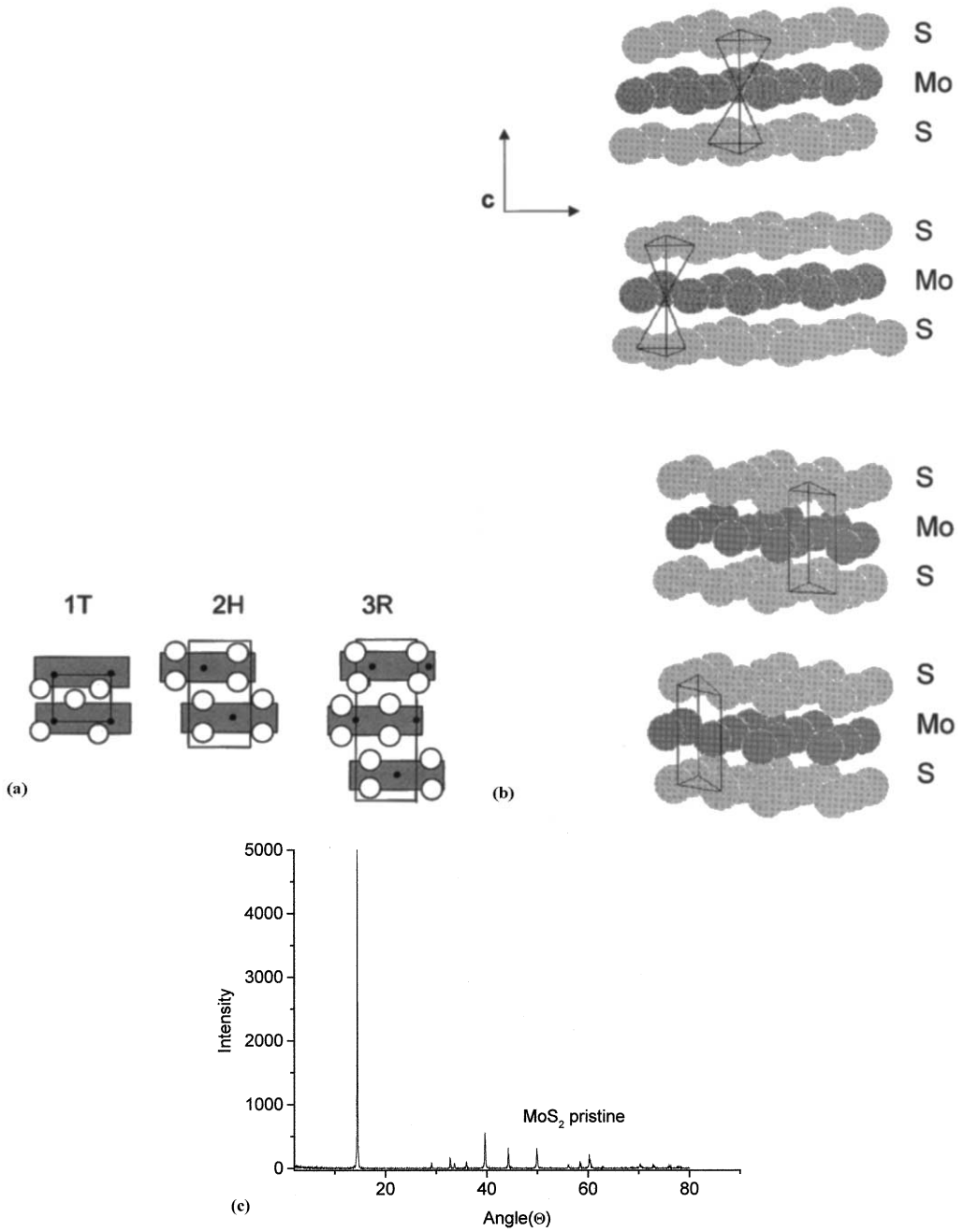

Fig. 1. (a) Projections of common polytypes for MoS_2 [110]. (b) Schematic representation of hexagonally closed packing MoS_2 layers and octahedral and trigonal prismatic local molybdenum coordination. (c) Powder X-ray diffraction pattern of 2H-MoS_2.

All MoS_2 modifications have, as shown schematically in Fig. 1b, a modulated structure consisting of S–Mo–S sandwich layers. Within the layers, each molybdenum atom is coordinated by six S-atoms in either a trigonal prismatic or octahedral (for 1T-MoS_2) arrangement by strong S–M–S bonds, while van der Waals bonds connect the nearest layers. So these materials are easy to slip or break by simply 'pulling off' the MoS_2 layers. Scanning tunneling microscopic images of natural and synthesized MoS_2 allow the resolution of two distinct atomic sites [35], one corresponding to the top hexagonal layer of sulfur atoms with a lattice constant of 3.16 Å and the other to an identical hexagonal lattice of Mo immediately below this plane and laterally displaced relative to the top layer. This agrees with the well-known X-ray crystal structure of the two alternating S–Mo–S sandwiches separated by a van der Waals gap along which cleavage occurs [36] (Fig. 1c).

2.3. Properties

2.3.1. Anisotropy

Physical and physicochemical properties, applications and importance of MoS_2 mostly arise from its laminar nature. Its properties are therefore markedly anisotropic, similar to those of graphite. Thus, for instance, MoS_2 is a highly anisotropic semiconductor displaying an electrical resistivity in the direction perpendicular to the planes about 1000 times greater than in the parallel direction (parallel resistivity, ca. 10 Ω cm) [37]. As will be discussed below, the MoS_2 intercalation compounds, in which special ordering of the intercalants are usually found, display similar properties.

2.3.2. Reactivity

As will be discussed later in this paper, MoS_2 may act in the intercalation processes as a reservoir of both electric charge and chemical species. Nevertheless, this sulfide behaves as a rather chemically inert substance [38]. Thus, etching using a standard solution of hydrochloric acid, nitric acid, or sulfuric acid leads to very rare or no incidence of holes on the surface after a normal etching time. Only a solution of sulfuric acid with potassium dichromate was found to create large and deep defects on the MoS_2 (0001) faces [38]. Resistance against photocorrosion in solution, useful for photoelectrochemical applications (vide infra), has also been observed [39]. Such a feature was originally attributed to the fact that the optical transition responsible for the creation of the electron–hole pairs is between non-bonding metal d states [40]. However, later detailed band structure calculations [8] have shown that in these chalcogenides the relevant state at the top of the valence band is not a non-bonding metal d state, but rather an antibonding state between metal d_{z^2} and non-metal p_z orbitals. This antibonding character is believed to be responsible for the high stability of this material against photocorrosion.

2.3.3. Catalysis

Molybdenum disulfide, in its various forms is of great interest in several catalytic reactions. The importance of MoS_2 as a catalyst lies not only in its relatively high activity, which for a given process could be not so large than the other metallic derivatives, but in its resistance to poisoning with sulfur [41].

The catalytic properties of the molybdenum sulfide are, as mentioned above, closely related to the structural properties of the material. Research in this area has focused mainly on two kinds of processes: dark electron transfer processes as hydrogenation activity and hydrogen evolution; and photochemical processes. Electrochemical studies show that the former occurs in the absence of light at centers located in the plane parallel to the *c*-axis, while the photoreactions occur on the van der Waals planes [42]. This is probably because the contributions of the non-bonding orbitals d_{z^2} or antibonding $d_{z^2}-p_z$ orbitals, forming the valence band, are located toward the van der Waals surface, while the orbitals which form the conduction band ($d_{x^2-y^2}$, d_{xy}, d_{xz}, d_{yz} and np_y) are oriented towards the surface parallel to the *c*-axis.

The hydrogenation of CO, methanation, has been used as a model reaction for testing catalysts from exfoliated MoS_2 [43]. High-activity catalysts are achieved when the single molecular layers of MoS_2, deposited onto a high surface area and doped with a nickel salt, is calcinated and reduced. However, the most active species appears to be an oxisulfide. Even in the absence of nickel as the promoter, the catalysts prepared by exfoliation show activities which are at least comparable to those prepared by precipitation from ammonium heptamolybdate [44]. Single layer MoS_2-based, alumina-supported catalysts, prepared by the inclusion of the aluminum species between MoS_2 layers, display a catalytic activity for the reaction of methanation rather higher than those obtained by the coprecipitation method [45].

MoS_2, like many molybdenum compounds, catalyses some chemical hydrogenation processes. It has in fact been used as the chief constituent or as a minor component in commercial catalysts. Silica- or alumina-supported MoS_2 has been applied widely in petrochemistry, namely as an active catalyst for removing sulfur and nitrogen from crude oil [46–51] (Eq. (1)). Product ratio depends on the hydrogenation activity of the catalyst [52–54].

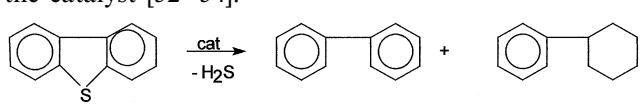

(1)

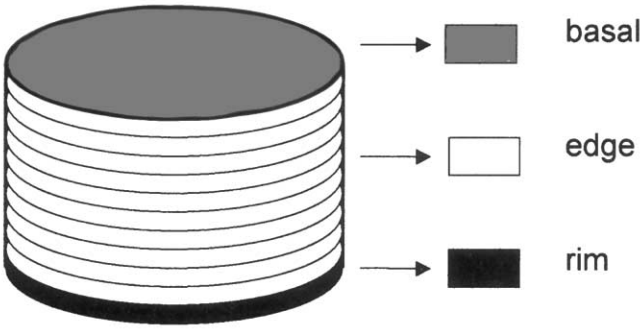

Fig. 2. 'Rim-edge' model for catalytic activity of MoS_2 (adapted from Ref. [57]).

The knowledge about the nature and position of the active sites in MoS_2-based catalysts has been an important problem for many years [55]. A cluster approach of active sites in MoS_2 catalysts using differential functional theory (DFT) calculations has been reported [56]. Most stable configuration corresponds to a flat absorption of a molecule of thiophene on the edge of the MoS_2 sheet. An interesting approach is the 'rim-edge' site model in which the MoS_2 catalyst particle is described as a stack of several discs [57]. There, the activity of unsupported MoS_2 is related to the coexistence of two different sites, which are directly dependent on the morphology of the MoS_2 crystallites, and more precisely, on the stacking height of the layers, see Fig. 2. The hydrogenation reaction is found to be catalyzed predominately by rim sites, while edge sites catalyze sulfur removal. The nature of the MoS_2 — pristine, exfoliated or delaminated — would be certainly important for determining the catalytic activity of this material. In fact, MoS_2 in alumina-supported catalysts obtained by conventional preparation techniques is mostly formed by the single layer sheets [58]. Supported single layer MoS_2, prepared by the exfoliation of Li_xMoS_2 and deposited on γ-alumina, is stable under the hydrodesulfurization reaction conditions, showing catalytic activity and selectivity similar to those of an alumina-supported multilayer MoS_2 catalyst [59].

Many commercial catalysts, however, consist of γ-Al_2O_3-supported molybdenum disulfide promoted by Co or Ni. In the application of MoS_2 as a catalyst for hydrodesulfuration (HDS), the intercalation of these promoter elements may result in improved catalytic activity. Features relevant to hydroprocessing reactions over MoS_2-supported catalysts promoted by Co or Ni have been recently reviewed [60]. The structure and active sites in unpromoted and promoted MoS_2-based HDS catalysts have been studied by self-consistent density functional theory. Comparison with the catalytic activity results for MoS_2, Co–Mo–S, Ni–Mo–S, and Fe–Mo–S shows that the highest activity is obtained for the structures with the lowest metal–sulfur binding energy [61]. An interesting approach for studying the influence of the promoter in the catalytic activity of MoS_2 is the preparation of intercalation compounds containing the promoter in the interlaminar spaces. Recently, the $Co_6S_8(PPh_3)_x$-pillared MoS_2 system in which the Co-cluster, as observed by TEM, can either intercalate into the bulk or bind to defect sites at edges of MoS_2, has been reported [62]. HDS and TEM results suggest that the role of Co in sulfide Co–Mo catalysts is to trop apart the MoS_2 layers, creating a higher percentage of rim sites and thus enhancing the hydrogenation capability. The structural characterization and behavior of MoS_2 intercalated with various proportions of $Co(OH)_2$ or Cp_2Co^+ ($Cp = C_2H_5$) as well as the use of these products as catalyst precursors for HDS of thiophene in a differential reactor have also been reported [63,64].

Silica-supported MoS_2 is also highly active for hydrogen evolution. Its activity in V^{2+} solutions is similar to that of the dispersed platinum [52]. Like in the hydrogenation reactions mentioned above, the catalytically active sites in hydrogen exchange reactions are located mainly on planes parallel to the c-axis, while the van der Waals planes remain inactive [65–67]. MoS_2 is sensitive to the presence of hydrogen. In fact, it has also been reported [68] that highly oriented films of MoS_2 on Al_2O_3 substrates, prepared with exfoliated disulfide in the form of single layers in suspension (vide infra) change their electrical conductivity when exposed to hydrogen gas, making them suitable for use in the fabrication of hydrogen gas sensors. The conductivity change is enhanced many times when Pt or Pd catalysts are dispersed onto the surface of the films. The effect of doping apparently arises from a Pt to Mo electron donation, with the formation of strong crystal field Mo–Pt bonds [69] by the displacement of a sulfur atom, and reduction of Mo^{+6} to Mo^{+5}. The mechanism of the conductivity change is probably related to the chemisorption of hydrogen molecules on the surface, followed by an electron transfer from the absorbed atoms to the conduction band of the n-type polycrystalline semiconductor MoS_2 film. The adsorption/desorption of hydrogen is probably a fast reaction. High efficiency and reproducibility of the single layer MoS_2 is certainly related to the fact that they have well-defined sites which are easy to oxidize, the layer edges, and sites that are passive, the basal planes.

2.3.4. Optical properties and photochemistry

MoS_2 is an indirect band gap material with the lowest indirect band gaps of 1.23 and 1.69 eV, respectively, as determined by photocurrent measurements in an electrochemical cell [70]. The electronic spectrum of bulk MoS_2 consists of a series of absorption thresholds (Fig. 3). The first threshold corresponds to the weak

absorption in the near infrared at about 1040 nm associated with an indirect gap between the top of the valence band at Γ and the bottom of the conduction band halfway between Γ and K in the Brillouin zone (Fig. 4). The second threshold, observed at about 700 nm, corresponds, as established by the results of the electronic band structure calculations, to the smallest direct transition at the point K of the Brillouin zone [71,72]. The two sharp peaks (A and B) on the high-energy site of the threshold are exitonic transitions whose energy separation of about 0.18 eV is because of the spin–orbit splitting of the top of the valence band at the K point. Direct transitions from deep in the valence band to the conduction band appear to give rise to both, to a third threshold at about 500 nm associated to two exitonic features in the spectrum (C and D), and to a fourth threshold at about 350 nm (E). The shape of the spectrum is variable as the relative intensity of the peaks A–E depends on the quality and the thickness of the sample.

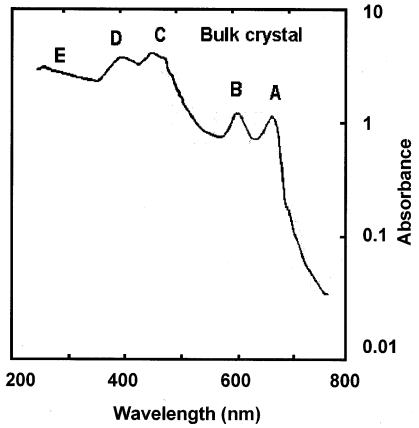

Fig. 3. Optical absorption spectrum of bulk MoS_2 (adapted from Refs. [72,73]).

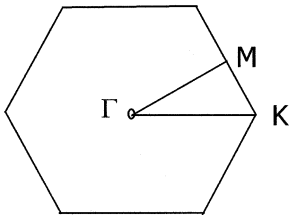

Fig. 4. Brillouin zone for hexagonal MoS_2.

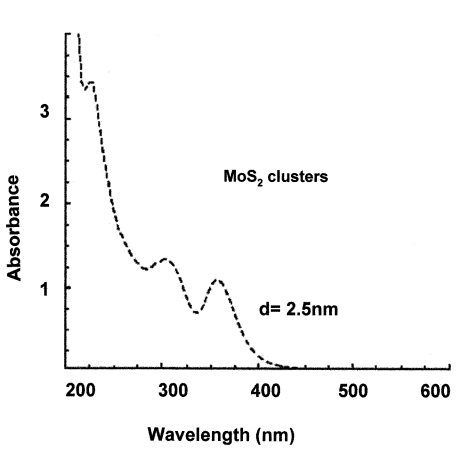

Fig. 5. Optical absorption spectrum of MoS_2 confined as 2.5 nm clusters (adapted from Ref. [73]).

Properties as well as the photochemical applications of MoS_2 are strongly related to the nature of the gap. The discussion as to whether the semiconducting gap in MoS_2 results either from the combined effect of the ligand field splitting and d–d hybridization of the Mo 4d orbitals or from an effect of metal-d–non-metal-p, appears to be resolved by calculations carried out later [8,71]. It was actually found that in the molybdenum dichalcogenides the Γ_4^- state at the top of the valence band is not a non-bonding metal d state, but rather an antibonding state between metal d_{z^2} and non-metal p_z orbitals. The corresponding bonding state is located about 5 eV below the top of the valence band, pointing to a large covalent interaction between the molybdenum d_{z^2} and ligand p_z orbitals. The antibonding nature of the band gap explains the high stability of these materials to photocorrosion.

Similarly to other semiconductors, the optical absorption and photoluminescent properties of MoS_2 may be modulated by controlling the particle size at the nanoscale. Size-selected nanosize clusters of molybdenum disulfide are obtained inside inverse micelles formed by the suspension of surfactant molecules dispersed in a non-polar continuous medium. From the reaction of molybdenum(IV) halide, dissolved inside the cages, with a metal sulfide or H_2S also as an inverse micelle solution, clear suspensions varying in color from near colorless for the smallest clusters to deep blue for the larger ones are obtained [73]. Using different sized micellar cages to encapsulate the molybdenum salt regulates the cluster size. The products may be purified further chromatographically [74]. The main structural features of bulk MoS_2 as determined by powder X-ray diffraction analysis remain intact in the encapsulated state at least for 4.5 nm diameter clusters [73]. However, the confinement causes large changes in the absorption spectrum of MoS_2. As can be seen in the spectrum reproduced in Fig. 5, although the main absorption features observed for bulk MoS_2 (see Fig. 3) remain essentially unaltered, large blue shifts with decreasing cluster size are induced. Interestingly, the spectra reveal that there is a one-to-one correlation between the bulk and cluster spectra, which persist at least for the clusters in the 3–2.5 nm size ranges. The theory predicts the existence of the crossover from solid-like to molecule-like optical absorption spectrum as the radius of the clusters became smaller than that of the exiton's Bohr radius in the bulk. However, for the MoS_2, it is

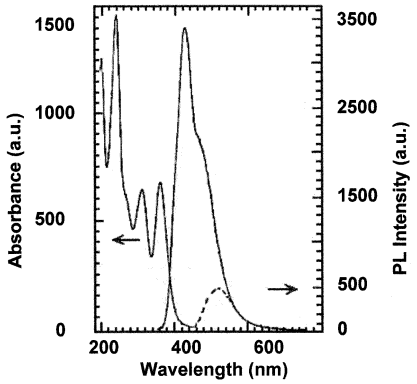

Fig. 6. Photoluminescent spectrum of 3 nm MoS_2 clusters (adapted from Ref. [74]).

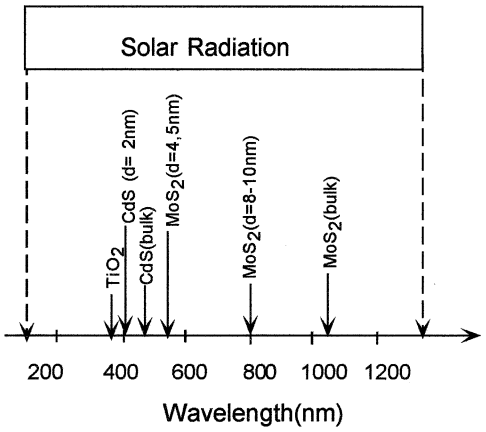

Fig. 7. Spectral range of solar radiation and absorbance edge of some semiconductor compounds (adapted from Ref. [39]).

apparent that clusters, which are only two unit cells thick, have sufficient densities of states to reproduce bulk-like absorption properties [74]. The changes in the shifts of the features seen in the optical absorption spectra of MoS_2 clusters is, according to the Effective Mass theory [75], proportional to $1/2\mu R^2$ where μ is the reduced mass of the exiton. The absorption spectra of fullerene like that of MoS_2 in the range of 400–800 nm, at temperatures between 4 and 300 K, and the influence of the size and the number of atomic layers, n, have been reported [76]. The semiconductivity of 2H-MoS_2 is preserved. However, reds shifts are observed in the A and B exiton energies for $n > 6$. However, blue shifts arising from quantum confinement in the z direction are observed for $n < 5$.

Photoluminescent (PL) phenomena, characteristic of semiconducting materials are also observable for MoS_2. Photogenerated electrons may undergo recombination directly with originated holes or may participate in recombination processes with trap or surface states. The latter processes are particularly probable in disordered layered solids as well as in nanoclusters, where there are a large number of atoms in or near the surface leading to a preponderance of dangling bonds and defects which may give rise to surface states. Impurities may play a similar role. In MoS_2, the often-observed photoluminescence takes place at energies lower than any of the absorption thresholds, and it is therefore dominated by surface recombination [74]. However, if purified MoS_2 nanoclusters are used, spectra of higher quality and photoluminescence features characteristic of both direct as well as surface e–h recombination may be observed. Thus, in PL spectra of purified 3.0 nm MoS_2 clusters, characteristic features at 520 and 420 nm, assignable to a surface and to the direct band edge recombination, respectively, are observed (see Fig. 6).

The luminescent properties of MoS_2 nanoclusters may also be modulated by modifying the surface of the clusters. Thus, the controlled deposition of gold, which does not change the wavelength but the intensity of the emissions, reduces the recombination process. Efforts have also been made to induce electron transfer to electron acceptors, namely 2,2′-bipyridine or 4,4′,5,5′-tetramethyl-2,2′-bipyridine, adsorbed on the MoS_2 nanoclusters [77]. The energetics of the reaction and therefore the dynamics of the electron transfer may be modulated by changing the electron acceptor or by varying the size of the MoS_2 cluster. Interesting experiments have also been carried out exploring the use of MoS_2 for catalyzing the photooxidation of organic chemicals. The oxidation potential of bulk MoS_2 is not large enough to produce hydroxide radicals (OH); however, quantum size effects on the band gap induce shifts of both the valence band and the oxidation potential of the semiconductor, thus permitting its catalytic activity [39].

The properties of MoS_2 discussed above, particularly the high photoresistance and the tunability of its absorption and photoemission features constitute interesting advantages of this semiconductor with respect to other materials such as CdS and TiO_2 which are usually mentioned in photochemical applications. Thus, for instance, CdS, in contrast with MoS_2, has band gap orbitals whose alteration severely affect the stability of the Cd–S bonds, making this material sensitive to photodegradation in water solutions [78]. Comparison with some wide-gap, photostable oxides such as TiO_2 also results favorably from the point of view of the use of solar energy for photoprocesses [79,80]. As illustrated in Fig. 7, because of its rather high band gap, TiO_2 can harvest only a small fraction of the solar spectrum. In contrast, MoS_2 can be photochemically active over a wide range, from about 1040 to $\sim$400 nm depending on the state of confinement in which the material has been prepared, thus covering a large part of the solar spectrum. Therefore, such properties make molybdenum disulfide a promising candidate for efficient solar energy cells [81,82]. Further, its high chemi-

cal durability, even in the presence of concentrated electrolytes, acids and strong oxidants in solution, and in general its high stability against photocorrosion when used as electrodes in photocells [40], as well as the 10% efficiency found for n-MoS_2-based photocells for Cl-oxidations or its use in photoanodes for SO_2 oxidation in a 6 M sulfuric acid medium, have made the molybdenum(IV) sulfide the subject of extensive electrochemical and photoelectrochemical studies [42,70,81,83–87].

2.3.5. Lubricant properties

The chemical inertness mentioned above, in addition to the weak van der Waals bonding between the layers characteristic of MoS_2, makes it useful for diverse applications as a solid lubricant in many space and terrestrial applications [88]. Thus, for instance, it is an excellent solid lubricant for high-precision space-borne uses such as satellite bearing, gears, and gimbals operating under extreme temperatures ranges [89–91], as well as in microsystems, where the effects of surface forces are more significant than those of gravity [92]. MoS_2 and other solid lubricant films necessary for such sophisticated applications may be obtained by both pulse laser deposition (PLD) [93–96], and magnetron sputtering [97,98].

2.3.6. Further technical applications

In addition to its catalytic ability and its properties as a lubricant, MoS_2 also makes to be an interesting material for battery operation [99]; especially when intercalated with Li, it has outstanding properties with potential applications for electrochemical energy storage [10,99–101]. Electrochemical features related to these applications will be discussed in the next section. Moreover, after the intercalation of alkali metals, MoS_2 transmutes from semiconductor to metal [102] also showing in some cases the existence of superconducting phase transitions [103]. The ability of MoS_2 for intercalating organic species which has been developed in recent years and will be reviewed Section 3, opens up the possibility of formulating several new materials, an example of which is the intercalation of liquid crystals in the lattice [104,105].

3. Intercalation of lithium

The intercalation of alkali metals into transition metal dichalcogenides is especially relevant both to fundamental knowledge and to technical applications of layered materials. This is particularly valid for MoS_2, as a great part of its intercalation chemistry is based on processes related to matrix lithiation. Although some research on the intercalation of alkali metals into MoS_2 has been reported [102–106], much attention has been focused on the intercalation of lithium, among others because of the potential of such materials as components of high power rechargeable batteries mentioned above.

The intercalation of an alkali metal like lithium into layered molybdenum disulfide may be described as an ion–electron transfer topotactic reaction. The electrons from the lithium (guest) are transferred to the lowest-lying unoccupied energy levels of the MoS_2 (host), which are principally transition metal d bands (see Fig. 8).

Such a description implies a host structure playing a rather passive role, supplying only host sites and redox centers. However, the intercalation actually may also induce important structural changes in the host. The nature of the products, the magnitude of the charge transfer, the structural and thermodynamic changes associated with the intercalation, as well as the reactivity of intercalates and the diffusion of the guest species in the interlaminar spaces are important questions on this topic.

3.1. Synthesis

Lithium may be intercalated into MoS_2 by both chemical and electrochemical methods. Currently, the chemical method used more frequently for intercalating lithium in transition metal dichalcogenides is the reaction of a suspension of the chalcogenide in an inert solvent of moderate boiling point with butyllithium [107] (Eq. (2)).

$$MS_2 + BuLi \rightarrow Li_xMS_2 \quad (2)$$

A near stoichiometric reaction may be normally achieved by refluxing the suspension of the reactants

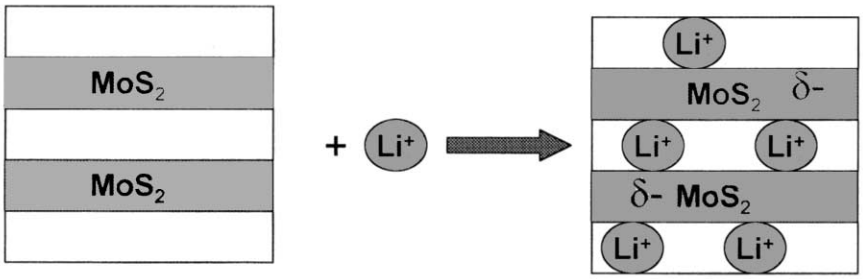

Fig. 8. Schematic representation of intercalation of lithium into MoS_2.

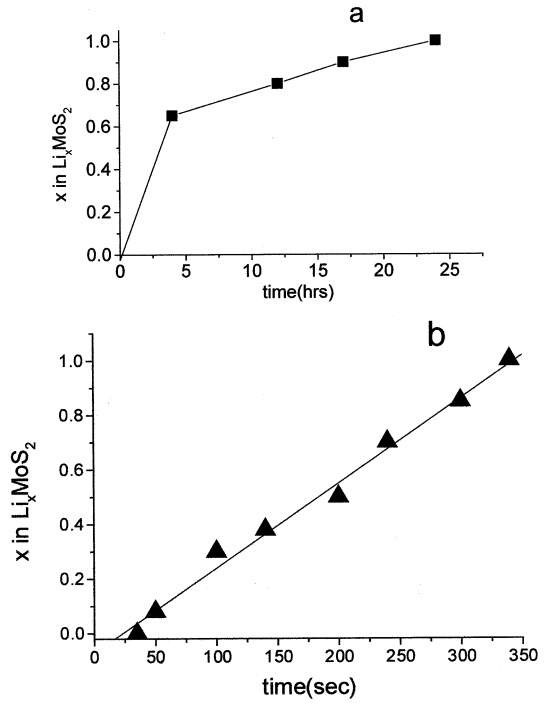

Fig. 9. Lithium intercalation degree as a function of reaction time for: (a) conventional thermal treatment; (b) microwave activation method [108].

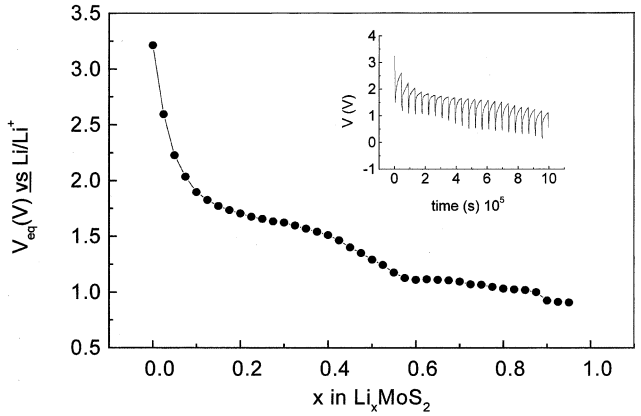

Fig. 10. Quasi-equilibrium voltage–composition curve for the intercalation of lithium into Li_xMoS_2. In the insert, voltage–time curve for the stepwise lithium intercalation in the range $0 < x < 0.6$.

for a couple of hours. However, MoS_2 appears to be rather inert to this reaction. In contrast with other transition metal disulfides as TiS_2, which may be easily intercalated, MoS_2 intercalates need about 24 h to reach an appreciable intercalation degree, often affecting the crystallinity of the products. However, Microwave assisted reactions make it possible to avoid long reflux times and to obtain good quality products [108]. A comparison of both methods (conventional thermal treatment and microwave intercalation) may be found in Fig. 9. The acceleration observed for microwave-assisted processes appears to be related to mechanistic changes that facilitate a first-stage intercalation enhancing the diffusion of lithium into the matrix.

3.2. Electrochemical behavior

Electrochemical intercalation is carried out by the electrolysis of a lithium salt with a non-coordinative anion solution in a non-aqueous solvent with a MoS_2 cathode. A typical electrochemical cell is Li(metal) | 0.5 M $LiClO_4$ in propylene carbonate | MoS_2 [109]. Although relatively, long times are required to obtain significant amounts of the product, the method has appreciable advantages. The intercalation may be quantitatively followed by coulometry and thermodynamic and kinetic information may be obtained easily (vide infra). Fig. 10 shows a typical voltage–composition curve for the intercalation of lithium in 2H-MoS2. In earlier reports on lithium intercalation into polycrystalline 2H-MoS_2, it was assumed that a decomposition reaction occurs at $x > 0.2$ forming Li_2S and metallic Mo [9,103,110]. Later, the dominant view has been that the products of the Li insertion into $2H_b$-MoS_2 actually correspond to the intercalation compounds Li_xMoS_2 [101,111–115]. Further, several authors suggest a phase transition from trigonal prismatic structure, 2H-MoS_2, to the octahedral structure, 1T-MoS_2, which would be stable at $x = 0$ and 1, respectively [100,112]. Within the intermediate range of x, both phases coexist [112].

3.3. Spectroscopic and structural features

In addition to the electrochemical information, X-ray diffraction analysis and vibrational spectroscopy have been often used to characterize the intercalation products as well as to understand the intercalation process. Further evidence has also been obtained from X-ray photoelectron spectroscopy, electron microscopy, X-ray absorption spectroscopy and theoretical calculations. Most of the evidence available now points to a phase change corresponding to the translation of atomic layers in the 2H-MoS_2 structure which changes its symmetry around molybdenum, leading to the 1T-MoS_2 phase with octahedral slabs.

The experimental Raman scattering spectrum results for lithium intercalated 2H-MoS_2 have also been interpreted using lattice dynamics models for pure 2H-MoS_2 and MoS_2 intercalated with lithium at different levels [116]. The model used for the 2H-MoS_2 lattice dynamics calculations is a three-spring central force model with the force constant scheme and the results reported in Table 1. The force constants required for producing the frequency of 205 cm^{-1} observed between the Li and the S atoms after intercalation are $A_{Li} = 12.12$ N m^{-1} and $B_{Li-S} = -0.88$ N m^{-1}. The main features

of the Raman spectrum of pure 2H-MoS_2, space group D^4_{6h}, are the E^1_{2g} mode at 383 cm^{-1}, the A_{1g} mode at 407 cm^{-1}, a small peak of the E_{1g} mode, and the rigid layer mode E^2_{2g} at 32 cm^{-1}. After intercalation with lithium, the Raman spectra show drastic changes [117]. Four main features are indeed observed. (i) A new Raman peak, at about 205 cm^{-1}, corresponding to an intercalation mode in which the lithium atoms vibrate strongly against the host lattice. (ii) New broad bands at about 1370 and 1600 cm^{-1}, observed by both Raman scattering and IR absorption, which appear to be caused by the vibrations of defects in the host lattice induced by the presence of lithium. (iii) The rigid layer mode, characteristic of the weak van der Waals binding force in MoS_2 at 32 cm^{-1} decreases in intensity as the lithium content increases, and this agrees with the breakage of the S–S bond across the van der Waals gap and its replacement by a S–Li–S bond. (iv) New weak, broad Raman peaks around the rigid band (RB) mode and on the low-frequency side of the E_{2g} and A_{1g} 2H-MoS_2 modes, which have been interpreted as arising from the formation of superlattice structures along the c axis.

Table 1
Binding energies of Li(1s) electrons [146]

Compound	E_b (eV)
$LiBF_4$	59.9
LiF	59.7
LiCl	58.1
LiBr	56.8
LiOH	58.7
Li_2CO_3	56.7
$LiNH_2$	55.8
$Li_{0.8}MoS_2$	55.6
Li(metal)	55.5

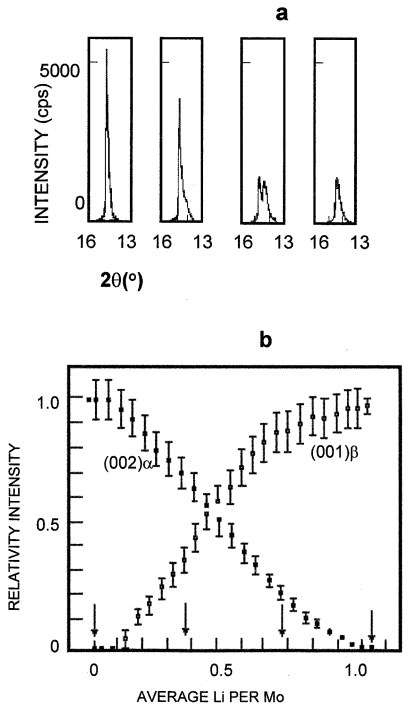

Fig. 11. (a) X-ray diffraction profiles of the cathode during lithium intercalation. (b) Contribution of 2H-MoS_2 peaks observed as a function of the lithium composition in the cathode. The arrows indicate the composition at which the profiles shown in (a) were taken [112].

In agreement with previous results indicating that at RT alkali metals can be intercalated into MoS_2 without changing the trigonal prismatic coordination of the host up to a limit of $x > 0.2$ [103], XPS results suggest the existence of 2H-Li_xMoS_2 for low x. However, a growing part of a new phase with an increasing lithium dosage is also observed [118]. Binding energies of Mo 3d core levels, a 3/2 and 5/2 photoemission doublet, are shifted to lower values by about 1.1 eV because of the increasing coverage of lithium. The lithium deposition shifts the Mo 3d core levels toward the position of the metallic Mo, but the same trend is also observed in the S 2p emission, which also increases with an increasing Li dosage. The observed shift of the Mo 3d and S 2p core level lines to lower binding energies (BE) during Li deposition on single crystals of MoS_2 can be also explained by the 2H → 1T phase transition. As the BE values of solids are referred to the position of the Fermi energy level (FE) in the solid, the measured BE will be lower for the 1T phase by the downward shift of the conduction band level and thus of FE.

The first systematic studies on the structural effect of the intercalation of lithium into MoS_2 were carried out using an electrochemical cell allowing the in situ X-ray diffraction analysis of the intercalated Li_xMoS_2 formed in the cathode. The results suggested that the 2H-MoS_2 lattice undergoes a first-order phase transition in which the coordination at Mo changes from a prismatic to an octahedral 1T-structure [112] leading to the phase distribution reproduced in Fig. 11. This phase transition was confirmed by using a highly crystalline Li_xMoS_2 prepared from Li_2S and Mo at high temperature [111]. The lithium content in the Li | Li_xMoS_2 intercalation cell varied in the range of $0 < x < 1.0$ while the in situ determination of the crystal lattice parameters showed that in this range there are several distinct phases with crystal lattices with small distortions from 1T-hexagonal symmetry [111]. During the conversion of 2H-MoS_2 into 1T-MoS_2 by electrochemical intercalation of lithium, cointercalation of the solvent molecules during the first discharge process may occur. However, if chemically prepared 1T-MoS_2 is used, the incorporation of the solvent may be avoided [119].

Electron diffraction studies carried out with Li_xMoS_2 prepared by the reaction of single crystal specimens of 2H-molybdenite with butyllithium throw some light on the nature of the distortion observed in the 1T-MoS_2

polytypes [120]; thus it was determined that in this species the MoS_2 layers are transformed into a distorted 1T-MoS_2 structure with the formation of a superlattice in the *a* and *b* directions. Such a distortion was assumed to be caused by the positions of the Li atoms in the interlaminar spaces. Much recently, a Mo–K edge EXAFS study for $Li_{0.85}MoS_2$ confirmed the existence of an intralayer distortion in the Mo-atom positions [63]. Two different Mo–Mo interatomic distances of 2.94 and 3.65 Å as well as a range of Mo–S distances were determined.

3.4. Single layer and restacked MoS_2

A number of studies have been made to resolve the structure of single-layer MoS_2 prepared by the exfoliation of Li_xMoS_2 in water. All of them have shown that the hydrolysis products retain the distorted 1T-MoS_2 structure found for the lithium intercalates discussed above. However, the products are the metastable species that undergo irreversible phase transitions back into 2H-MoS_2 on heating or aging [31,63].

Raman spectra of single layer MoS_2 contain strong features at 156, 226 and 333 cm^{-1} that are absent in spectra obtained from 2H-MoS_2. Specially interesting to follow is the Raman mode at 383 cm^{-1} from 2H-MoS_2, which should be active in a single layer trigonally prismatic coordinated MoS_2, but inactive in single layer octahedrally coordinated MoS_2. Thus, the decomposition of this phase may be estimated by either the absence or the relative intensity of this mode. Direct comparison of the Raman spectra with calculated phonon dispersion curves indicates that the experiments are consistent with the formation of a distorted octahedral structure [121].

These results agree with the X-ray pattern of the same material obtained in suspension in water. From the comparison of the experimental pattern with the patterns calculated considering single molecular layers with a distorted octahedral coordination, there are two different Mo–Mo bond lengths, supporting a superlattice which, among other possibilities, may be described as a $\mathbf{2}\boldsymbol{a} \times \mathbf{2}\boldsymbol{a}$ [122].

The EXAFS data indeed show that for similar samples there are two predominant Mo–Mo distances at 2.82 and 3.82 Å, which are shorter and longer, respectively, than the bulk 2H-MoS_2 *a*-spacing of 3.17 Å [123]. More recent EXAFS experiments [63] with restacked MoS_2 have lead to similar results, namely two Mo–Mo distances of 2.77 and 3.79 Å. Combining the *a* and *b* lattice parameters measured from electron diffraction patterns with the Mo–Mo and Mo–S distances calculated from Mo–K edge EXAFS spectra, a $\mathbf{2}\boldsymbol{a} \times \mathbf{2}\boldsymbol{a}$ superstructure is obtained in which the ideal 1T-MoS_2 structure is distorted by the formation of trinuclear Mo clusters with a Mo–Mo bond length of 2.77 Å [63].

The superstructure of restacked MoS_2 has also been resolved recently from electron diffraction data on small single crystal domains. Patterson projections obtained from the two-dimensional *hk*0 data indicate univocally that the metal atoms are distorted to form a zig-zag chain with a short Mo–Mo distance of 2.92 Å [124]. MoS_2 has a $\mathbf{2}\boldsymbol{a} \times \boldsymbol{a}$ superstructure that can also be described by an orthorhombic $\sqrt{\mathbf{3}}\boldsymbol{a} \times \boldsymbol{a}$ cell. The observed distortion resembles the structure of the WTe_2 [125]. In addition, for restacked MoS_2, diffraction patterns pointing to $\mathbf{2}\boldsymbol{a} \times \mathbf{2}\boldsymbol{a}$ superstructures are often observed [126]. However, such features could be produced by the superposition of three $\sqrt{\mathbf{3}}\boldsymbol{a} \times \boldsymbol{a}$ crystals rotated 120° relative to each other because of a twining phenomenon [124].

The major differences between the thermodynamically stable 2H-MoS_2 and metastable 1T-MoS_2 may be illustrated by the following model [31,127]. The fully reduced MoS_2 lattice is isoelectronic with the binary sulfides of the Group VIIB elements like ReS_2. While 2H-MoS_2 provides a trigonal prismatic environment for the metal cations, the addition of one more electron as in ReS_2 or in fully reduced $[MoS_2]^-$ leads to distorted octahedral environment with a significant change in the band structure and in the electrochemical potentials. The $[MoS_2]^-$ configuration can be obtained via the thermal preparation of the ternary phase $KMoS_2$ [126]. The oxidation of the latter at 300 K does not result in the formation of 2H-MoS_2 but yields 1T-MoS_2. STM studies of the totally oxidized product lead to the superstructure $\sqrt{\mathbf{3}}\boldsymbol{a} \times \sqrt{\mathbf{3}}\boldsymbol{a}$ [128]. Moreover, by the incomplete oxidation of $K_x(H_2O)_yMoS_2$ the following sequence could be recognized: K_zMoS_2, $z \approx 0.7$ $(\mathbf{2}\boldsymbol{a} \times \mathbf{2}\boldsymbol{a}) \rightarrow K_z(H_2O)_yMoS_2$, $z \approx 0.3$ $(\boldsymbol{a} \times \sqrt{\mathbf{3}}\boldsymbol{a}) \rightarrow K_z(H_2O)_y$-$MoS_2$, $x < 0.3$ $(\boldsymbol{a} \times \mathbf{2}\boldsymbol{a}) \rightarrow$ 1T-MoS_2 $(\sqrt{\mathbf{3}}\boldsymbol{a} \times \sqrt{\mathbf{3}}\boldsymbol{a})$ [128].

3.5. Theoretical considerations

The comparison of the intercalation chemistry of transition metal disulfides as TiS_2, TaS_2 or ZrS_2 with that of the MoS_2 shows some marked differences. Thus, the development of the chemistry of MoS_2 has occurred rather later than that for other transition metal disulfides. The reason for this delay should to be found in the electronic structure of the MoS_2. From a theoretical point of view, the change from a stable prismatic phase to a metastable octahedral phase, mentioned above, is an instance of a clearly identifiable problem. Any model describing the electronic structure of MoS_2 should explain both the reaction conditions under which the conversion occurs and the structures of these phases.

The simplest approach to understanding the electronic structures of both 2H- and 1T-MoS_2 consists in analyzing the ligand field splitting experienced by the Mo 4d orbitals in a trigonal-prismatic and an octahe-

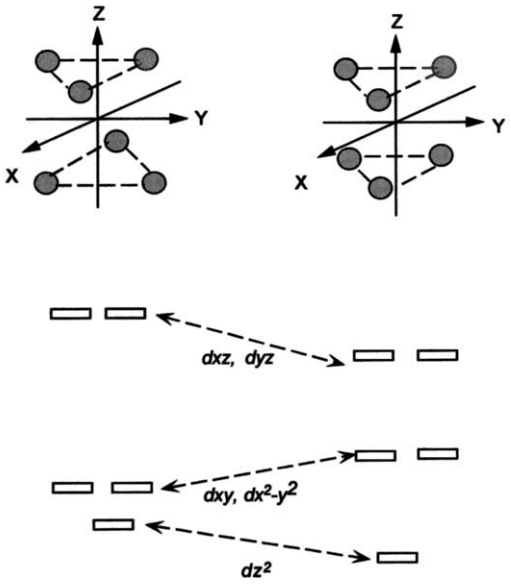

Fig. 12. Ligand field splitting of Mo-d orbital in octahedral and trigonal-prismatic environments.

dral environment, respectively (Fig. 12). Taking the z-axis to be colinear with the three-fold axis in a trigonal-prismatic polyhedron, the sulfur ligands lying in or near the nodal cone of the d_{z^2} orbital should be non-bonding. The orbitals more strongly directed to the ligands, the d_{xz} and d_{yz} pairs, will have the more Mo–S antibonding character, while the $d_{x^2-y^2}$ and d_{xy} orbitals will undergo an intermediate interaction with the sulfur atoms. In the case of octahedral coordination, taking the C_4 axis to be coincident with the z-axis, the well-known splitting pattern of the e_g and t_{2g} groups is found. For a d^2 electron configuration, the trigonal-prismatic arrangement is more stable.

The density of states (DOS) distributions calculated using the extended Hückel method indicates that the splitting pattern is conserved (Fig. 13). There are a number of electronic structure calculations on 2H-MoS_2. The main concern in all of them is the nature of band gap. As a first approximation, it may be considered that above the sulfur p-bands there are three peaks which correspond to the $d_{z^2} < d_{x^2-y^2}$, $d_{xy} < d_{xz}$, d_{yz} arrangement expected from the ligand field splitting diagram. However, in many calculations a considerable mixing is detected between the levels d_{z^2} and ($d_{x^2-y^2}$, d_{xy}), with some sulfur p-character also, which for the valence band could be, for instance, about 40, 44, and 16%, respectively [129]. For the conduction band a similar mixing is found. Different attempts to describe the electronic structure of MoS_2 have involved either the band [130,131], or the ligand-field [132,133] approaches. Models and calculations performed with ab initio [8] as well as empirical methods have arrived at similar results. Only acknowledging an extended state mixing, experimental features such as diamagnetism, semiconductivity with a band gap around 1 eV, and photo-resistance, mentioned earlier, may be explained.

It is also interesting to mention that, analyzing the Mo–Mo crystal orbital–population curves, weak Mo–Mo bonds in 2H-MoS_2 have been detected. Moreover, Mo–Mo bonding supporting an extended hexagonal metal–metal bonded network would be an important factor stabilizing the structure. Such an interaction also gives rise to orbital splitting and the corresponding band gap, similar to that of the pristine d_{z^2} and $d_{x^2-y^2}$, d_{xy} set. The gap then separates groups of bands, which are weakly Mo–Mo bonding and antibonding [129,134].

In the band structure for compounds like 1T-MoS_2, there are, beyond six bands with a strong sulfur p-char-

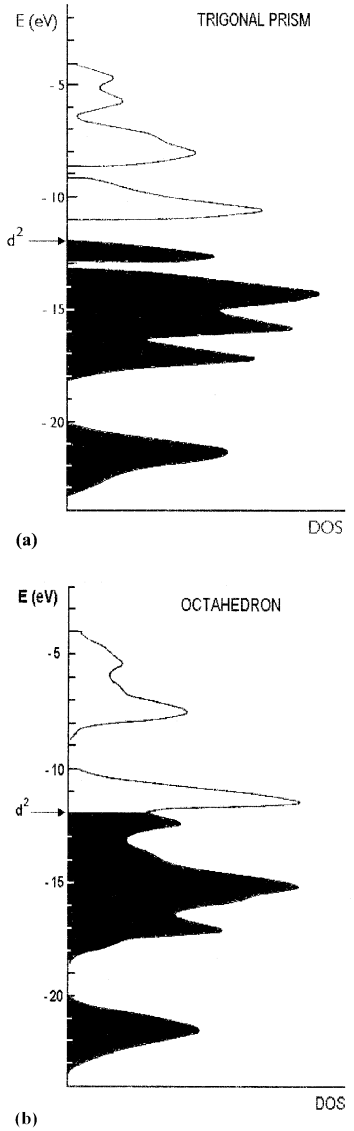

Fig. 13. DOS distributions for MoS_2 with trigonal-prismatic (a) and octahedral (b) molybdenum coordination (adapted from Ref. [135]).

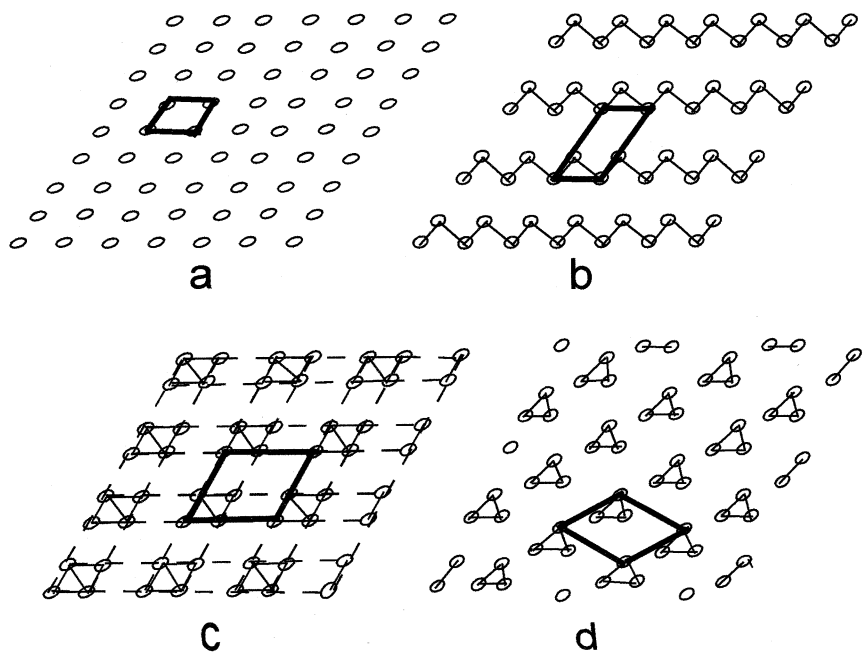

Fig. 14. Types of distortions and superstructures in layered d^2 and d^3 transition-metal compounds with octahedral coordination. (a) Undistorted ($\boldsymbol{a}$); (b) chain formation ($\boldsymbol{2a} \times \boldsymbol{a}$); (c) diamond shape ($\boldsymbol{2a} \times \boldsymbol{2a}$); (d) triangular clustering ($\sqrt{\boldsymbol{3a}} \times \sqrt{\boldsymbol{3a}}$).

acter, three bands, which correspond to the metal containing the t_{2g} block. However, not fully in accord with the simplified picture based on crystal field arguments, a contribution of the d_{z^2} and other orbitals should also be considered. The Fermi level for a d^2 species lies in the middle of the valence band, so that the products are expected to display the metal properties. The comparison of the two kinds of layers, trigonal-prismatic versus octahedral, by carrying out the energy band structure calculations using a RB model indicates clearly that for a d^2 configuration the trigonal-prismatic structure is preferred [135]. However, by the addition of one electron, i.e. in d^3 complexes such as ReS_2, the octahedral coordination becomes more favorable.

1T-MoS_2 is a CdI_2-type transition-metal compound formed by MoS_2 layers made up of MoS_2 edge-shared distorted octahedra. As discussed above, the products obtained are metastable species, which present superstructures that often depend on the procedure used for their synthesis. The concepts and theoretical approaches related to the trends in preferring a particular solid-state geometry as well as structural modulations in layered transition-metal dichalcogenides like those observed for MoS_2 have been the subject of numerous reviews [135–137]. Lattice distortions produced by clustering are explained on the basis of both the local chemical bonding [136,137] and hidden Fermi surface nesting [136,138] concepts. Factors such as the electron counting and the length of metal–ligand bonds, metal–metal bonding and lattice strain are crucial in determining the pattern of metal–atom clustering favored by a given system.

For layered transition-metal compounds of octahedral coordination with d^2 and d^3 electron counts, different metal–atom clustering patterns have been observed, Fig. 14. Zig-zag chains are apparent in some 1T-ML_2 layers containing d^2 ions such as $MoTe_2$ and WTe_2 [125]. In 1T-ML_2, as discussed above, $\sqrt{\boldsymbol{3a}} \times \sqrt{\boldsymbol{3a}}$ superstructures, which may be interpreted as a weak trimerization of the metal atoms, are observed [128]. For d^3 1T-ML_2 compounds such as ReX_2 (X = S, Se) there is a metal–metal diamond-chain formation [139,140]. The driving force causing such distortions from the regular geometry arises from an energy gap in the Fermi level introduced by clustering. In solid-state physics, such a process is associated to the Fermi-surface-nesting concept which in terms of molecular chemistry corresponds to a first-order Jahn–Teller instability, i.e. the tendency of partially filled degenerate levels to undergo a distortion which lifts the degeneracy [136]. In the case of 1T-ML_2 structures, the t_{2g} block bands of the layer may be approximated as a superposition from three sets of edge-sharing chains. Thus, the structural modulations of 1T-ML_2 with different electron counts are explained using solid-state physic concepts by the hidden 1D Fermi surfaces arising from such a superposition. For this approach, only the σ-bonding interactions undergone by the in-plane t_{2g} orbitals within each edge-sharing octahedral chain are considered. Structural modulation of 1T-MoS_2 may be explained from the point of view of local chemical bonding by considering, in the case of diamond chain (d^3) and zig-zag chain (d^2) formation, a two-center

two-electron σ-bonding [136] (see. Fig. 14). However, the energetics of the structure modulation in 1T-MoS_2 compounds depends, as mentioned above, on a number of factors which prevent the generalization of these observations. In the case of the 1T-MoS_2, a structure modulation by the formation of triatomic clusters giving rise to a $\sqrt{3}a \times \sqrt{3}a$ superstructure is seen often [128]. In fact, band structure calculations have shown that the metal–atom trimerization in this species lowers the total energy and opens a band gap for a very small displacement of the metal atoms. This trimerization would be the way in which species with relatively short M–L bond lengths, such as the MoS_2, can stabilize the system avoiding large lattice strain. The fact that the type of clustering depends on a series a relatively subtle factors such as M–M bonding and lattice strain, both related, in turn, to the M–L bond length and the electron populations, explains why in the case of 1T-MoS_2 the observed distortions from an ideal octahedral structure depend strongly on the history of the material.

Theoretical models explaining the intercalation process in these materials are mainly based on the band theory calculations within the RB approach [141]. There, a complete electron transfer leading to Li^+ ions inserted in an anionic layered matrix $(MS_2)_n^-$ is assumed [142]. According to this approach, voltage variation with lithium composition as described in Fig. 10 is often explained by using a gas lattice model [99,143]. In such a model, the change in free energy is associated to the formation of lithium ions in an interlaminar lattice of sites according Eqs. (3) and (4)

$$V = E_0 + gU_x + k_B T \ln\left[\frac{x}{(1-x)}\right] \quad (3)$$

$$\frac{dx}{dV} = -\left(\frac{dx}{dV}\right) e^{-1} = \left[gU + \frac{k_B T}{(1-x)x}\right]^{-1} \quad (4)$$

where E_0 is the energy associated to the filling of an isolated lattice site; U, the ionic interaction energy between intercalated atoms; g, the number of sites coupled to a given site; and, a last term, considering the configurational entropy, with k_B and T as the Boltzmann's constant and the absolute temperature, respectively.

In spite of the success of the band theory for describing long-range periodic interactions in the solids, the major part of the lattice electronic structure is determined by local environments formed by the reduced arrangements of atoms [144]. It is not possible to discuss the specific bonding, guest–host interactions or ionic diffusion within the RB approach, i.e. the case of some experimental evidences indicating that the charge transfer involved in the intercalation process could be partial. Thus, for instance, according to ^{7}Li-NMR chemical shifts in $LiTiS_2$ [145], the $Li \rightarrow TiS_2$ charge transfer actually reaches only about 80%. In the case of MoS_2, as shown in Table 1, X-ray photoelectronic spectroscopy experiments indicate that the transfer is only partial [146]. Such a fact should be reflected in the actual oxidation state of the transition metal in the lattice, which is mainly determined by the local environment of the guest. However, there are methods from quantum chemistry, the molecular orbital (MO) and density function (DFT) theories that are helpful to describe such systems [133]. A theoretical model based on quantum mechanical calculations of $(TiS_2)_n$ clusters has been developed [147,148]. There, the system is described by the electron chemical potential, μ_{el}, which is seen as a natural property of the system. In the context of the DFT, $-\mu_{el}$ corresponds to the value of the absolute electronegativity changes in the lattice [149], which in turn, may be expressed as a function of the charge Q acquired by the system. Thus, in a first-order approach, $\chi(Q)$ is given by Eq. (5)

$$\chi(Q) = \chi^0(Q=0) + Q\left(\frac{\partial\chi}{\partial Q}\right)_{Q=0} \quad (5)$$

where, the first term is the host electronegativity, while the second term describes a progressive decrease in χ with an increasing guest–host charge transfer. The synergic effect which leads to the partial charge transfer mentioned above is described in Fig. 15. This description, derived originally for TiS_2, is appropriate for explaining the influence of the Li environment in MoS_2 intercalates on the variation of the charge capacity and the electrode voltage as a function of the degree of intercalation [150,151].

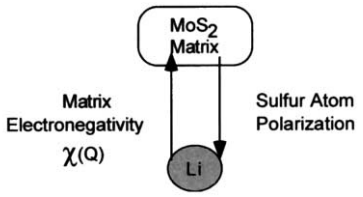

Fig. 15. Scheme for the host–guest charge exchange in MoS_2 [151].

4. Intercalation of molecular species

4.1. Intercalation of donor compounds into MoS_2

The insertion of molecular guest species into the interlaminar spaces of MoS_2 leads, analogously to other layered solids, to intercalation compounds. However, owing to the inertness of the MoS_2 matrix mentioned earlier, achievements in this field have required special experimental procedures.

Synthesis work may be classified according to the methods used for assisting the intercalation reactions.

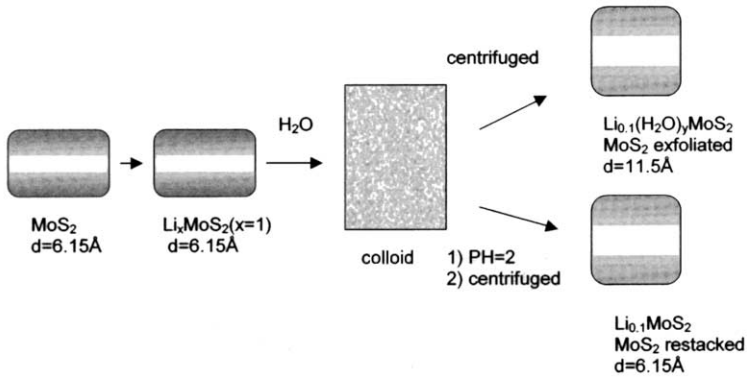

Fig. 16. Exfoliation of $LiMoS_2$.

Table 2
Types of guests intercalated into MoS_2 by exfoliation methods

Type of guest	Matrix activation method	Examples of host–guest products	References
Polymers	Exfoliated and restacked	$Li_{0.1}MoS_2(PEO)_y$ ($y = 1$–1.3)	[165,166]
Molecular donor	Exfoliated	$Li_{0.1}$ MoS_2 $(HNR_2)_y$ ($y = 0.11$–0.41)	[170]
Cationic species	Exfoliated	$(R_4N)_xMoS_2$ ($x<1$)	[160,162]
Organometallic species	Restacked	MoS_2[(arene)$Ru(H_2O)_3$]	[182]

The following methods may be identified clearly: (i) electrochemical deposition of lithium [152]; (ii) formation of monolayer colloids in water [153,154]; (iii) reaction with electropositive metal in liquid NH_3 [155]; and (iv) reduction with butyl lithium in non-aqueous media [156]. The existence of a step in which the matrix is reduced is a common feature in these methods. The formation of single-layer colloidal solutions by matrix exfoliation have been by large the most widely used procedure.

4.2. The exfoliation method

MoS_2 avoids direct intercalation, except for lithium. However, using the property of many layered solids of allowing single-layer suspensions in water, a very efficient method has been developed. The rapid hydrolysis of Li_xMoS_2 produces molecular hydrogen causing the exfoliation of the sulfide [157].

The exfoliation process is not a purely mechanical process, but a chemical one in which the lithiated matrix is partially oxidized leading to a polyanion $[(MoS_2)^{-x}]_n$. A negative charge on the monomolecular layers definitely leads to the formation of a colloidal alkaline suspension. The suspension is a black laminar product that contains about 10% mol lithium and water, probably corresponding to the formula $Li_x(H_2O)_yMoS_2$. This 'exfoliated MoS_2' has an interlaminar distance of about 11.5 Å [155]. As shown in the scheme in Fig. 16, the colloidal solution may also be alternatively flocculated by the addition of acid. At ca. pH 2 it is possible to separate a product which has the same interlaminar distance as pristine MoS_2, but which is rather more reactive to intercalation than the latter [158,159]. This product is normally known as 'restacked MoS_2' and corresponds, as discussed above, to 1T-MoS_2. Suspensions of either exfoliated or restacked products may be used for the intercalation of a series of inorganic, organic or organometallic species [159–161] (vide infra).

The addition of a variety of organic compounds, dissolved in water-unmiscible solvents, to a suspension of exfoliated disulfide leads to flocculation of the colloid. The products may be described as the result of the insertion of a layer of the organic species in the interlaminar spaces of the molybdenum disulfide. This method, first proposed for depositing exfoliated MoS_2 on alumina particles [68], has been used for obtaining a number of intercalation products. The variety of MoS_2 intercalation products obtained by this method may be visualized in the examples mentioned in Table 2.

4.3. Intercalation of polymers

Macromolecules can also be intercalated into MoS_2 by the exfoliation method. In fact, a number of both saturated and conjugated polymers have been inserted in the van der Waals interlaminar spaces of this matrix [163–165]. The intercalation into exfoliated MoS_2 is essentially a topotactic process, in which only changes in the interlaminar distances are apparent. In general, the diffraction patterns of the intercalated products

show intense 00*l* reflections, indicating that they have preferentially ordered layered structures. The d-spacing and interlayer expansions, besides elemental and thermal analysis as well as other product properties, often provide relevant information about the characteristic of the polymeric interlaminar phase. Selected examples of this kind of compound are listed in Table 3. These systems in which both organic and inorganic phases are molecularly compatible can be considered as nanocomposites; and, consequently, they may in principle exhibit a variety of unique properties different from those obtainable by merely mixing the two components. Structural and electronic changes in the host produced by intercalation often induce drastic changes in the transport properties of the MoS_2, turning it, for instance, from a semiconductor to a metallic material. Great emphasis has been placed, therefore, in the study of systems in which the ionic and/or electronic conducting properties may be improved. The intercalation of polyethers such as the poly(ethylene oxide) (PEO) widely used as the basis for solid electrolytes, has been intensively studied [166–168]. Many efforts have also been made in the intercalation of electronic conducting polymers as polypyrrole [163] and polyaniline (PANI) [164]. The intercalation of polyaniline dissolved in *N*-methylpyrrolidinone was accomplished using single layer MoS_2 [164]. A layer expansion of 4.2 Å was seen. A different procedure has been utilized for the insertion of polypyrrole (PPY) into MoS_2 [163]. The compound $MoS_2(PPY)_{0.24}$ was prepared by oxidizing an aqueous solution of single MoS_2 layers and pyrrole with $FeCl_3$. By a stepwise addition of the latter to the pyrrole–MoS_2 mixture both events, polymerization of the pyrrole and precipitation of polymer–MoS_2 nanocomposite, occur simultaneously. As a consequence of polymer growth under kinetically restricted conditions, the intercalated polymer has a relatively low molecular weight. The polymer is obtained in its doped form. Although the authors prefer to assume that the doping anion should be the OH^- ion, further evidence discussed in this paper, showing that the exfoliated MoS_2, alone as well as in many of its intercalation products, appears to present a negative charge, makes the MoS_2 host by itself a good candidate as the dopant anion of the intercalated polypyrrole. The compound is a p-type semiconductor, and its conductivity is similar in magnitude to that of $MoS_2(PANI)_{0.35}$ [164].

Table 3
Selected examples of intercalation of polymers into MoS_2

Compound	Lattice expansion (Å)	References
$(PEO)_{0.92}MoS_2$	10.1	[164,166]
$(PPG)_{0.5}MoS_2$	9.2	[164]
$(PVP)_{0.76}MoS_2$	14.9	[164]
$(Mcel)_{0.26}MoS_2$	14.2	[164]
$(PEI)_{0.83}MoS_2$	4.0	[164,168]
$(Nylon\text{-}6)_{3.6}MoS_2$	11.3	[164]
$((CH_2\text{-}n)_3MoS_2$	4.1	[164]
$(PANI)_{0.35}MoS_2$	4.2	[164]
$(PPY)_{0.24}MoS_2$	4.5	[163]

Abbreviations. PEO: poly(ethylene oxide); PPG: poly(propylene glycol); PVP: poly(vynilpyrrolidinone); Mcel: methyl cellulose; PEI: polyethyleneimine; PANI: poly(aniline); PPY: polypyrrole.

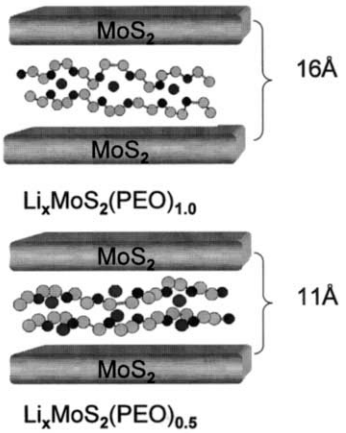

Fig. 17. Intercalation of PEO into MoS_2.

The intercalation of PEO has been the most widely studied system. The nanocomposites are in general prepared by the exfoliation method. The affinity of these polyethers to intercalation appears to be high enough to allow PEO–MoS_2 intercalation ratios around 1:1. These reactions depend more on the intercalation procedures than on the polymer molecular weight. The products are always layered species with interlaminar distances in the range of 11.5–16 Å. Among the diversity of reported PEO–MoS_2 products, it has been possible to separate, depending on the reaction conditions, two well-defined pure phases. One of them $Li_{0.1}MoS_2(PEO)_{0.5}$ with an interlaminar distance of 11.5 Å corresponds to the insertion of a monolayer of the polymer. As illustrated in the scheme in Fig. 17, in the case of the compound $Li_{0.1}MoS_2(PEO)_{1.0}$, the increase in the interlaminar spaces is owing to the intercalation of the two polymer layers with an interlaminar distance of 16 Å. However, in both cases, about the same lithium content is found [169].

4.4. Intercalation of molecular donors

Although the insertion of amines in layered solids may be considered as a typical intercalation reaction, only those examples of intercalation of amines in MoS_2 included in Table 4 have been reported [170]. However, the observed interlaminar distances and amine–MoS_2 intercalation ratios indicate, that the geometrical model considering the van der Waals volumes of the guest, which is often used for explaining the experimental

Table 4
Molybdenum dsulfide dialkylamine, $Li_{0.1}MoS_2(HNR_2)_y$ [170]

Amine HNR_2	Guest–host (mol/mol)	Lattice expansion (Å)
Diethylamine	0.42	3.74
Dibutylamine	0.19	3.90
Dipentylamine	0.11	4.04
N-Isopropylcyclohexylamine	0.21	4.26
Dicyclohexylamine	0.21	4.45

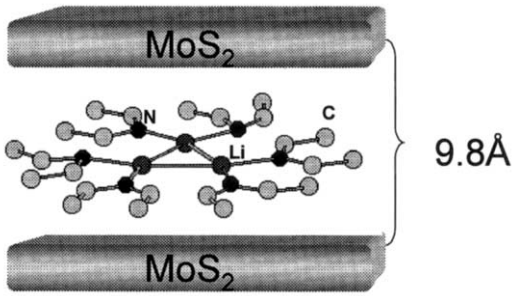

Fig. 18. Self-assembling of a trinuclear lithium cluster induced by intercalation of diethylamine into MoS_2 [171].

interlaminar distances, at least in this case, fails. Structural and elemental analysis data can be understood only by considering a contraction of the guest induced by the intercalation. Recently it was observed, that in the compound $Li_{0.1}MoS_2(Et_2NH)_{0.2}$ a self-assembling of a trinuclear lithium cluster in the interlaminar space occurs [171]. The schematic structure shown in Fig. 18 was deduced both from the magnetic second moments $M(^7Li–^7Li)$, $M(^7Li–^1H)$ and $M(^1H–^1H)$ seen in the NMR spectrum of the compound at low temperatures, and from the correlation between the volume of the guest corresponding to observed stoichiometric ratio and the space — MoS_2 molecular surface and interlaminar distances — available in the host. The intercalation of phenantroline has also been achieved by the exfoliation method [160]. Two phases containing, respectively, 0.31–0.35 and 0.1 mol phenantroline per mole of MoS_2, with interlaminar distances of 14.92–15.56 and 9.7 Å, respectively, have been isolated. The reaction conditions necessary for obtaining these phases, specifically pH-values low enough for stabilizing the protonated phenantroline, appear to indicate that, in this case, the guest is the cationic species.

From the reaction of an aqueous suspension of exfoliated MoS_2 and naphthalene in dichloromethane, followed by reflocculation at pH 2, a series of compounds with the formula $MoS_2(C_{10}H_8)_x(H_2O)_y$ where x and y are in the ranges of 0.07–0.20 and 0.05–0.28, respectively, has been obtained. The stoichiometry of the product depends on the stirring time following acidification. After 14 days the product $MoS_2(C_{10}H_8)_{0.20}$-$(H_2O)_{0.19}$ with an interlaminar distance of about 10.4 Å is obtained. The observed Δc value suggests that the plane of the aromatic species is parallel to the MoS_2 layers [172].

Molecular species of greater complexity and size, such as metal clusters, may be also intercalated in MoS_2 [173]. The addition of CH_2Cl_2 solution of the $Co_6Q_8(PR_3)_6$ (Q = S, Se, Te) cluster to a suspension of exfoliated MoS_2 leads to the formation of the intercalation compounds $MoS_2[Co_6Q_8(PR_3)_y]_x$ ($y = 3–6$ $x = 0.02–0.09$). The maximum d spacing of 21.5 Å found from the X-ray diffraction patterns of the material is consistent with the size of the intercalated cluster. The low intercalation ratios indicate that the host interlayer surface is only partially occupied, thereby leading to a 'pillared' arrangement of the guest. In fact, the BET surface area measurements indicate that these intercalation compounds display surfaces significantly higher than both the bulk and restacked MoS_2. However, TEM measurements indicate that the laminar expansion owing to the clusters is localized [174]. Further, these experiments reveal, that the interlayer distance may vary from the distances determined by X-ray diffraction (vide supra) to ca. 14 Å corresponding to a species from which the triphenylphosphine ligands have been completely removed. This effect might be induced by vacuum pumpdown during the TEM experiments. The intercalation of the aluminum cationic cluster $[Al_{13}O_4(OH)_{24}(H_2O)_{12}]^{7+}$ into MoS_2 has been accomplished using the single layer MoS_2. The products $MoS_2[Al_{13}O_4(OH)_{24}(H_2O)_{12}]_x$ with x in range of 0.02–0.05 and a typical expansion of about 9.9 Å do not contain any negatively charged species other than the apparently polyanionic matrix. According to the one-dimensional electron density mapping calculations, the cluster maintains its structural integrity while intercalated [175].

4.5. Intercalation of cationic species

The treatment of the MoS_2-colloidal solution with tetralkylammonium salts, R_4NX (X = Cl or Br) leads to the flocculation of the corresponding intercalation compounds [160,176]. The amount of the quaternary ammonium cations in these compounds is found to range from 0.15 to 0.30 per MoS_2 unit. As neither the halide nor the oxygen are detected, the authors came to the conclusion that the charge of the polyanion in the compounds $(NR_4)_xMoS_2$ are being exactly compensated by the cation, also ranging between -0.15 and -0.30, with the typical mean value of -0.25. These results are qualitatively consistent with the residual lithium content observed in the intercalation of polyethylene oxide and amines mentioned above.

The addition of a transition metal salt solution to a single layer MoS_2 dispersion results in the precipitation

of intercalation compounds which, in general, may be described by the formula $M_z(H_2O)_yMoS_2$. In these compounds, the content of the intercalated metal appears to depend on the charge of the M^{+n} cation used for precipitation. For various cations with $n = 2$, 3, and 4, z was found to correspond to $1/n$. For the divalent cations Fe^{2+}, Co^{2+} and Ni^{2+} respective values of $z = 0.50$, 0.55, and 0.56 were found. The negative charge necessary for compensating the charge of the intercalated cation — approximately one unit according to the $1/n$ relationship — appears to be distributed between both the MoS_2 layers and the OH^- ions. Specifically for precipitation with iron(II) sulfate, in which case the presence of Fe(II) and Fe(III) was detected, the formula $[Fe^{2+}_{0.25}Fe^{3+}_{0.35}(OH^-)(MoS_2)^{0.25-}]$ has been proposed [176,177]. Mo–K-edge extended X-ray absorption fine structure and X-ray near-edge structure studies of $M_{0.5}(OH)MoS_2$ (M = Mn, Co, Ni) intercalates indicate that the electronic structure and the environment of M atoms are similar to those in the crystalline hydroxides $M(OH)_2$ [178]. Further, in the Ni derivative data indicate that changes associated with an increasing electron density occur in the matrix sulfur atoms. In experiments related to the use of Li_xMoS_2 as a material for the extraction of aqueous heavy metal ions, the intercalation compounds $Hg_{0.50}MoS_2$ and $Pb_{0.15}MoS_2$ were isolated [179]. The selectivity of Li_xMoS_2 for the heavy metal ion was found to be $Hg^{2+} > Pb^{2+} > Cd^{2+} > Zn^{2+}$. The affinity for the ions in general increases when the extractions are carried out under anaerobic conditions. The compounds $(Co(OH)_2)_{0.27}MoS_2$ and $(Co(OH)_2)_{0.76}MoS_2$ were obtained from the flocculation of exfoliated MoS_2 in the presence of the precursors $(Co(OH)_2)_6(NO_3)_2$ and $(Co(NH_3)_6)Cl_3$ [63], respectively. According to the magnetic susceptibility measurements and EXAFS results, which in general agree with those mentioned above [180], indicate that the intercalated species actually correspond to the cobalt(II) hydroxide. However, the same work [63] describes the Mo–K-edge studies corresponding to a mixture of 1T-MoS_2 and 2H-MoS_2 structures.

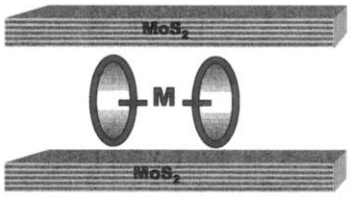

Fig. 19. Intercalation of metallocene into MoS_2 [181].

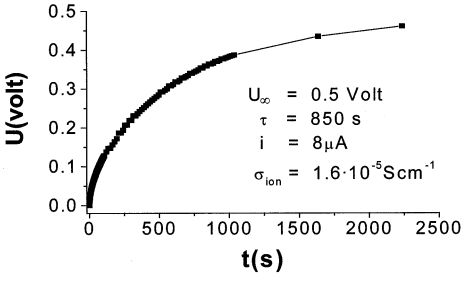

Fig. 20. dc Polarization curve for $Li_{0.1}MoS_2(dibutylamine)_{0.19}$ at 1 μA [170].

4.6. Organometallic species

The intercalation of ferrocene into MoS_2 has been achieved by treating a saturated CCl_4 solution of an organometallic compound with a single layer MoS_2 suspension in water [153,162]. According to a geometrical model, proposed earlier for explaining the intercalation of a series of metallocenes into other transition metal dichalcogenides, ferrocene is, as shown schematically in Fig. 19, preferentially oriented with its cyclopentadienyl rings perpendicular to the MoS_2 basal planes [181]. However, because of the rather low observed Fe–Mo ratios (mean value of ten experiments 0.054), this compound may be considered to have a pillared structure. Two phases have been obtained from the intercalation of $[(arene)Ru(H_2O)_3]^{2+}$ complexes (arene = C_6H_6, $C_6H_2Me_4$-1,2,4,5; C_6H_4Me-1-pr-4) depending on the reaction pH [182]. In an acid medium, pH 3.2, the ruthenium complex is inserted as a monomer, while at pH 8.5, the ruthenium is a binuclear species. Comparison of the interlayer distances with the expected geometry of the guest indicates that the arene ligands are also oriented roughly perpendicular to the MoS_2 slabs. More recently, the intercalation of the metallocene cations $[M(Cp)_2]^+$ (M = Fe, Co) were prepared by the flocculation of exfoliated MoS_2, prepared by the hydrolysis of $Li_{0.85}MoS_2$, with the respective metallocenium chlorides. The X-ray absorption data reveal products with alternating layers of metallocenium guest ions and partially negatively charged MoS_2 sheets. Further, the Mo–K-edge EXAFS indicates that both 1T- and 2H-type structures are present [63].

4.7. Transport properties

Besides conformational, thermal and spectroscopic changes in donor guests accompanying the intercalation, important changes in the transport properties of the host–guest compounds as a whole are often observed.

4.7.1. Electrical conductivity

As observed in the polarization curve of the compound $Li_{0.1}MoS_2(dibutylamine)_{0.19}$ shown in Fig. 20, MoS_2–donor composites behave as mixed electronic–ionic conductors [170]. Electronic conductivity, measured mostly by electrochemical impedance spec-

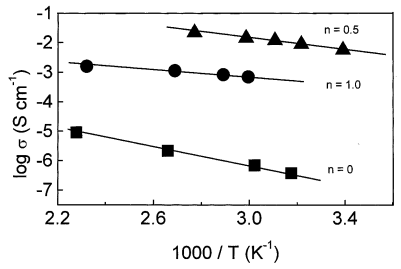

Fig. 21. Arrhenius plots for the electrical conductivity of MoS_2 (■); $Li_{0.1}MoS_2(PEO)_{0.5}$ (▲); and $Li_{0.1}MoS_2(PEO)_{1.0}$ (●) [183].

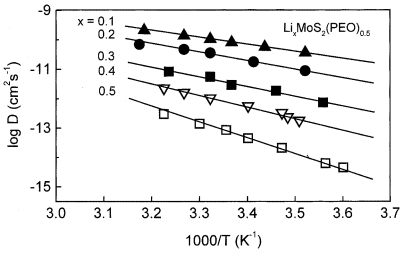

Fig. 22. Arrhenius plots for the diffusion of lithium in $Li_xMoS_2(PEO)_{0.5}$ at $x = 0.1$ (▲), $x = 0.2$ (●), $x = 0.3$ (■), $x = 0.4$ (▽) and $x = 0.5$ (□) [183].

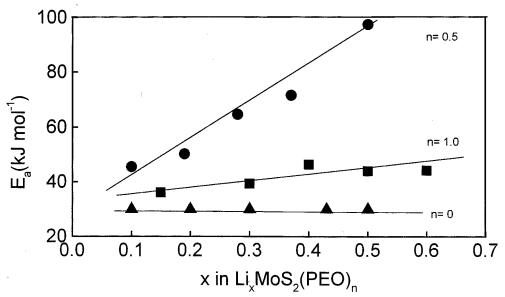

Fig. 23. Influence of lithium concentration in the activation enthalpies for the diffusion of lithium in PEO-based nanocomposites $Li_{0.1}MoS_2(PEO)_{0.5}$ (●), $Li_{0.1}MoS_2(PEO)_{1.0}$ (■) and in Li_xMoS_2 (▲) [185].

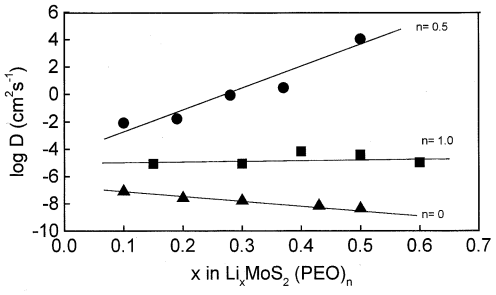

Fig. 24. Dependence of Arrhenius plot intercepts $\log D_{T=\infty}$ on x in the PEO-based nanocomposites $Li_{0.1}MoS_2(PEO)_{0.5}$ (●), $Li_{0.1}MoS_2(PEO)_{1.0}$ (■) and in Li_xMoS_2 (▲) [185].

troscopy, depends both on the lithium content and the nature of the interlaminar phase. As observed in the Arrhenius plots displayed in Fig. 21, MoS_2–PEO nanocomposite microcrystalline products behave as semiconductors [183]. Room temperature conductivities as high as 3×10^{-2} S cm^{-1} have been observed in the case of secondary amine intercalates mentioned above [170]. Rather high electrical conductivities have also been observed in the products of the intercalation of aluminum cationic clusters mentioned above [175].

4.7.2. Lithium diffusion

No detailed information on ionic conductivity in MoS_2 nanocomposites, which is estimated to be about 10% of the total conductivity, is available yet. However, relevant information about the migration properties of lithium ion in the interlaminar spaces has been obtained from lithium diffusion studies.

When lithium is cointercalated with a donor, diffusive properties are expected to be determined not only by the matrix, but also by the coordinative properties of the guest species. In the case of MoS_2 available information is related to the lithium diffusion in PEO-based nanocomposites, specifically from the study of the chemical diffusion coefficients of $Li_xMoS_2(PEO)_{0.5}$ and $Li_xMoS_2(PEO)_{1.0}$ determined by the galvanostatic relaxation technique [184] at different temperatures and lithium molar fractions [185]. Chemical diffusion coefficients depend both on the temperature and lithium content as well as on the nature of the nanocomposite. The dependence of D on the temperature often follows, as illustrated in Fig. 22, an Arrhenius behavior, from which information on the lithium diffusion thermodynamic activation parameters may be obtained (vide infra). Lithium diffusion coefficients increase with an increasing temperature but decrease with increasing lithium content. Nevertheless, lithium diffusion rates in PEO-containing phases are in general higher than in the pure MoS_2.

The influence of the donor cointercalation on the thermodynamic activation parameters of lithium diffusion as a function of lithium concentration is illustrated in Fig. 23. More or less linear relationships are always observed. The lithium diffusion activation enthalpies are higher for the PEO nanocomposites than for MoS_2. The dependence of D on x is determined by the nature of the interlaminar phase, and is particularly noticeable in the case of $Li_xMoS_2(PEO)_{0.5}$. Such differences, which may be also visualized from the dependence of log $D_{T=\infty}$. Arrhenius intercepts on x shown in Fig. 24, apparently arise from the influence of the coordination of the lithium ions in the interlaminar spaces on the diffusion mechanism. In agreement with the structural description of the MoS_2–PEO nanocomposites given above (see Fig. 17), in the case of both MoS_2 alone and $Li_xMoS_2(PEO)_{1.0}$, lithium maintains the same coordination in the whole range of x, while in the composite $Li_xMoS_2(PEO)_{0.5}$, such a coordination may change, altering the energy barrier to diffusion.

5. Conclusions

The most significant features of both applied and fundamental chemistry of molybdenum disulfide are strongly related to the layered nature of this compound. In fact, the traditionally more prominent applications of MoS_2, namely the lubricant properties and the catalytic use of the compound pure or promoted with other metal species, are both strongly dependent on the weak van der Waals intralaminar interactions and on the nature of the sites defined by its layered structure. Physicochemical properties of the compound are also determined by the same features. Optical properties of MoS_2 tridimensionally confined in spaces of the order of the nanometers show a behavior characteristic of quantum materials. Nonetheless, particles in the range of 2.5–3 nm diameter containing only a few layers are enough for retaining the electronic properties of the extended solid. The chemical behavior of MoS_2 is also dominated by the laminar nature of the solid, specifically by the insertion of chemical species into the intralaminar spaces as well as by the kinetic and thermodynamic factors affecting the intercalation processes.

Among the thermodynamic factors associated to the intercalation chemistry of MoS_2, the main one appears to be the electron band structure of the 2H-MoS_2 derived from the trigonal prismatic coordination of the molybdenum atom in the solid. A direct, electron transfer-assisted intercalation process would require the occupation of the empty conduction band of relatively high energy. The 2H-$MoS_2 \rightarrow$ 1T-MoS_2 phase transition overcomes such a hindrance. In the 1T-MoS_2, with a octahedral coordination of the molybdenum atoms, there is a partially filled conduction band which makes the redox processes associated with the intercalation more favorable.

However, phase change leads to a structural rearrangement, so the existence of an energy barrier makes the process kinetically difficult. Required synergism between the phase change and electron transfer associated with intercalation makes the system strongly dependent on the diffusion of the intercalated species in the MoS_2 matrix.

Strategies for successful intercalation are related to the improvement of both charge transfer and diffusion rates. Lithium species with high reduction potentials and high mobility are particularly appropriate for such purposes. Lithium intercalates in which lithium is found occupying the octahedral sites in the MoS_2 interlaminar spaces are thus used as precursors of other more complex intercalation compounds. Experimental procedures for optimizing the intercalation of lithium as well as for intercalating the donor species combine the reduction of the matrix with exfoliation processes making thus the intercalation both thermodynamically and kinetically possible.

The coordination of both molybdenum in the layers and lithium in the interlaminar spaces determine that MoS_2-based intercalation compounds are the mixed ionic–electronic conducting species with potential applications in the development of new materials useful in, among others, the fields of electronics, rechargeable batteries, and energy storage.

Acknowledgements

Research partially founded by FONDECYT (Grand 1981082), Fundación Andes (Grand C-12510), DID Universidad de Chile.

References

[1] R. Schöllhorn, in: J.L. Atwood, J.E.D. Davies, D.D. MacNicol (Eds.), Inclusion Compounds, vol. 1, Academic Press, London, 1984 (chap. 7).
[2] D. O'Hare, D.W. Bruce, D.S. O'Hare (Eds.), Inorganic Materials, Wiley, Chichester, 1992.
[3] D. Yoffe, Solid State Ionics 39 (1990) 1.
[4] E.P. Gianellis, Adv. Mater. 8 (1996) 29.
[5] R. Schöllhorn, Chem. Mater. 8 (1996) 1747.
[6] G.A. Ozin, Adv. Mater. 4 (1992) 612.
[7] G.A. Ozin, Chem. Commun. (2000) 419.
[8] R. Coehoorn, C. Haas, J. Dijikstra, C.J.F. Flipse, R.A. de Groot, A. Wold, Phys. Rev. B 35 (1987) 6195.
[9] M.S. Whittingham, Prog. Solid State Chem. 12 (1978) 41.
[10] M. Winter, J.O. Besenhard, M.E. Spahr, P. Novák, Adv. Mater. 10 (1998) 725.
[11] J.J. McKetta, in: J.J. McKetta, W.A. Cunningham (Eds.), Encyclopedia of Chemical Processing and Design, vol. 30, Marcel Dekker, New York, 1989.
[12] B. Elvers, S. Hawkins, G. Schulz (Eds.), Ullmann's Encyclopedia of Industrial Chemistry, vol. A16, VCH, New York, 1990.
[13] Kirk-Othmer, Encyclopedia of Chemical Technology, vol. 15, Wiley, New York, 1981.
[14] Th. Weber, J.C. Muijsers, J.H.C. van Wolput, C.P.J.- Verhagen, J.W. Niemantsverdriet, J. Phys. Chem. 100 (1996) 14144.
[15] K.I. Tanaka, T. Okuhara, Catal. Rev. Sci. Eng. 15 (1977) 249.
[16] R.R. Chianelli, M.B. Dines, Inorg. Chem. 17 (1978) 2758.
[17] D. Volllath, D.V. Szabo, Mater. Lett. 35 (1998) 236.
[18] E. Borsella, S. Botti, M.C. Cesile, S. Martelli, A. Nesterenko, Mater. Sci. Forum 636 (1998) 278–281.
[19] R. Bichsel, F. Levy, J. Phys. D: Appl. Phys. 19 (1986) 1809.
[20] M.S. Donley, N.T. McDevitt, T.W. Haas, P.T. Murray, J.T. Grant, Thin Solid Films 168 (1989) 335.
[21] M.S. Donley, P.T. Murray, S.A. Barber, T.W. Haas, Surf. Coat. Technol. 36 (1988) 329.
[22] G. Chatzitheodorou, S. Fiechter, M. Kunst, J. Luck, H. Tributsch, Mater. Res. Bull. 23 (1988) 1261.
[23] W.K. Hoffman, J. Mater. Sci. 23 (1988) 3981.
[24] J. Cheon, J.E. Gozum, G.S. Girolami, Chem. Mater. 9 (1997) 1847.
[25] R.S. Patil, Thin Solid Films 340 (1999) 11.
[26] Y. Feldman, E. Wasserman, D.J. Srolovitz, R. Tenne, Science 267 (1995) 222.
[27] D.J. Srolovitz, S.A. Safran, M. Homyonfer, R. Tenne, Phys. Rev. Lett. 74 (1995) 1778.

[28] Y. Feldman, G.L. Frey, M. Homyonfer, V. Lyakhovitskaya, L. Margullis, H. Cohen, G. Hodes, J.L. Hutchison, R. Tenne, J. Am. Chem. Soc. 118 (1996) 5362.
[29] M. Homyonfer, Y. Feldman, L. Margulis, R. Tenne, Fullerne Sci. Technol. 6 (1998) 1.
[30] C.M. Zelensky, P.K. Dorhout, J. Am. Chem. Soc. 120 (1998) 734.
[31] F. Wypych, R. Schölhorn, J. Chem. Soc. Chem. Commun. (1992) 1386.
[32] P. Jellinek, Nature 185 (1960) 376.
[33] B.W. Brown, D.J. Beersten, Acta Crystallogr. 18 (1965) 31.
[34] A.J. Jacobson, in: A.K. Cheetham, P. Day (Eds.), Intercalation Reactions of Layered Compounds, Oxford University Press, Oxford, 1992.
[35] M. Weimer, K.C. Bai, J.D. Baldeschwieler, Phys. Rev. B 37 (1988) 4292.
[36] R.G. Diickinson, L. Pauling, J. Am. Chem. Soc. 45 (1923) 1466.
[37] J.A. Wilson, A.D. Yoffe, Adv. Phys. 18 (1969) 193.
[38] J.R. Lince, P.D. Fleischauer, J. Vac. Sci. Technol. A 5 (1987) 1312.
[39] T.R. Thurston, J.P. Wilcoxon, J. Phys. Chem. B 103 (1999) 11.
[40] H. Tributsch, Z. Naturforsch. Teil A 32 (1977) 972.
[41] S.E. Moore, J.H. Lunsford, J. Catal. 77 (1982) 97.
[42] G.S. Calabrese, M.S. Wrighton, J. Am. Chem. Soc. 103 (1981) 6273.
[43] B.H. Miremadi, R. Morrison, J. Catal. 103 (1987) 334.
[44] G.A. Scholz, S.R. Morrison, Can. J. Chem. 67 (1989) 862.
[45] B.K. Miremadi, S.R. Morrison, J. Catal. 112 (1988) 418.
[46] J. Valyon, W.K. Hall, J. Catal. 84 (1983) 216.
[47] J. Valyon, R.J. Schneiden, W.K. Hall, J. Catal. 85 (1984) 277.
[48] K. Ramanathan, S.W. Weller, J. Catal. 95 (1985) 249.
[49] W.S. Millman, K.J. Segawa, D. Smrz, W.K. Hall, Polyhedron 5 (1986) 169.
[50] J.T. Richardson, J. Catal. 112 (1988) 313.
[51] E.G. Derouane, E. Pedersen, B.S. Clausen, Z. Gabelica, R. Candia, H. Topsoe, J. Catal. 99 (1986) 253.
[52] A. Sobczynski, J. Catal. 131 (1991) 156.
[53] M.S. Wittingham, R.R. Chianelli, J. Chem. Ed. 57 (1980) 569.
[54] T.A. Pecoraro, R.R. Chianelli, J. Catal. 67 (1981) 430.
[55] H. Topsoe, B.S. Clausen, Catal. Rev. Sci. Eng. 26 (1984) 395.
[56] P. Faye, E. Payen, D. Bougeard, J. Mol. Model 5 (1999) 63.
[57] M. Daage, R.R. Chianelli, J. Catal. 149 (1994) 419–427.
[58] S. Eijsbouts, G.C. VanLeerdam, Bull. Soc. Chim. Belg. 104 (1995) 347.
[59] W.P. Boone, J.G. Ekerdt, J. Catal. 193 (2000) 96–102.
[60] J. Grimblot, Catal. Today 41 (1998) 111.
[61] L.S. Byskov, J.K. Norskov, B.S. Clausen, H. Topsoe, J. Catal. 187 (1999) 109.
[62] J. Brenner, C.L. Marshall, L. Ellis, N. Tomczyk, J. Heising, M. Kanatzidis, Chem. Mater. 10 (1998) 1244–1257.
[63] K.E. Dungey, M.D. Curtis, E. Penner-Hahn James, Chem. Mater. 10 (1998) 2152–2161.
[64] K.E. Dungey, M.D. Curtis, E. Penner-Hahn James, J. Catal. 175 (1998) 129–134.
[65] D. Chadwick, M. Breysse, J. Catal. 71 (1981) 226.
[66] G.C. Stevens, T. Edmonds, J. Less-Common Met. 54 (1977) 321.
[67] K. Tanaka, T. Okuhara, J. Catal. 78 (1982) 155.
[68] B.K. Miremadi, R.C. Singh, S.R. Morrison, K. Colbow, Appl. Phys. A 63 (1996) 271.
[69] B.K. Miremadi, S.R. Morrison, J. Catal. 131 (1991) 127.
[70] K.K. Kam, B.A. Parkinson, J. Phys. Chem. 86 (1982) 463.
[71] R. Coehoorn, C. Haas, R.A. de Groot, Phys. Rev. B 35 (1987) 6203.
[72] R.F. Frint, A.D. Yoffe, Proc. R. Soc. London A 273 (1963) 69.
[73] J.P. Wilcoxon, G.A. Samara, Phys. Rev. B 51 (1995) 7299.
[74] J.P. Wilcoxon, P.P. Newcomer, G.A. Samara, J. Appl. Phys. 81 (1997) 7934.
[75] A.D. Yoffe, Adv. Phys. 42 (1993) 173–266.
[76] G.L. Frey, S. Elani, M. Homyonfer, Y. Feldman, R. Tenne, Phys. Rev. B: Condens. Matter Mater. Phys. 57 (1998) 666.
[77] F. Parsapour, D.F. Kelley, S. Craft, J.P. Wilkinson, J. Chem. Phys. 104 (1996) 4978.
[78] N. Serpone, P. Maruthamuthu, P. Pichat, E. Pelizzetti, H.J. Hidaka, J. Photochem. Photobiol. A: Chem. 85 (1995) 247.
[79] M.T. Hoffmann, S.T. Martin, W. Choi, D. Bahnemann, Chem. Rev. 95 (1995) 69.
[80] M.A. Fox, M.T. Dulay, Chem. Rev. 93 (1993) 341.
[81] A. Simon, A.J. Ricco, D.J. Harrison, M.S. Wrighton, J. Phys. Chem. 87 (1983) 4446.
[82] P. Pramanik, S. Bhattacharya, Mater. Res. Bull. 25 (1990) 15.
[83] H. Tributsch, H. Gerischer, C. Clemen, Ber. Bunsen-Ges. Phys. Chem. 83 (1979) 655.
[84] W. Kautek, H. Gerischer, H. Tributsch, J. Electrochem. Soc. 127 (1980) 2471.
[85] H. Tributsch, J.C. Bennett, J. Electroanal. Chem. 81 (1977) 97.
[86] C.P Kubiak, L.F. Schneemeyer, M.S. Wrighton, J. Am. Chem. Soc. 102 (1980) 6898.
[87] W. Kautek, H. Gerischer, H. Tributsch, Ber. Bunsen-Ges. Phys. Chem. 83 (1979) 1000.
[88] A. Schroeer, E. Pfluegen, Oberflaechen Polysurf. 40 (1999) 10.
[89] P.D. Fleischauer, J.R. Lince, P.A. Bertrand, R. Bauer, Langmuir 5 (1989) 1009.
[90] I.L. Singer, Mater. Res. Soc. Symp. Proc. 140 (1989) 215.
[91] H.E. Sliney, Tribol. Int. 15 (1982) 303.
[92] Y. Tian, G. Liu, Y. Hong, S. Fu, Y. Hu, Proc. SPIE-Int. Soc. Opt. Eng. 3512 (1998) 236.
[93] P.T. Murray, V.J. Dyhouse, L. Grzulis, D.R. Thomas, Mater. Res. Soc. Symp. Proc. 201 (1991) 513.
[94] M.S. Donley, P.T. Murray, N.T. McDevitt, Mater. Res. Soc. Symp. Proc. 140 (1989) 277.
[95] J.S. Zabinsky, M.S. Donley, P.J. John, V.J. Dyhouse, A.J. Safriet, N.T. McDevitt, Mater. Res. Soc. Symp. Proc. 201 (1991) 195.
[96] P.J. John, V.J. Dyhouse, N.T. McDevitt, A.J. Safriet, J.S. Zabinski, M.S. Donley, Mater. Res. Soc. Symp. Proc. 201 (1991) 117.
[97] B. Bellido, A.H.S. Jones, J. Hampshire, T.J. Allen, J. Witts, D.I. Teer, K.J. Ma, D. Upton, Surf. Coat. Technol. 97 (1997) 687.
[98] M.C. Simmonds, A. Saban, H Van Swygenhoven, E. Pfluger, S. Mikhailov, Surf. Coat. Technol. 108–109 (1998) 340.
[99] C. Julien, G.A. Nazri, Solid-State Batteries: Materials Design and Optimization, Kluwer Academic, Dordrecht, 1994.
[100] R.R. Haering, J.A.R. Stiles, K. Brant, US Patent N 4,224,390 (1980).
[101] F.C. Laman, M.W. Matsen, J.A.R. Stiles, J. Electrochem. Soc. 135 (1986) 2441.
[102] J.V. Acrivos, W.Y. Liang, J.A. Wilson, A.D. Yoffe, J. Phys. C 4 (1971) 418.
[103] R.B. Somoano, V. Hadek, A. Rembaum, J. Chem. Phys. 58 (1973) 697.
[104] M. Hara, Y. Iwakabe, K. Tochigi, H. Sasabe, A.F. Garito, A. Yamada, Nature 228 (1990) 344.
[105] D.P.E. Smith, W.M. Heckl, Nature 346 (1990) 616.
[106] W. Rudorff, Chimia 19 (1965) 489.
[107] M.D. Dines, Mater. Res. Bull. 10 (1987) 287.
[108] E. Benavente, G. González, Mater. Res. Bull. 32 (1997) 709.
[109] M.A. Santa Ana, V. Sánchez, G. González, Electrochim. Acta 40 (1995) 1773.
[110] M.S. Whittingham, J. Electroanal. Chem. 118 (1981) 229.

[111] P.J. Mulhern, Can. J. Phys. 67 (1989) 1049.
[112] M.A. Py, R.R. Haering, Can. J. Phys. 61 (1983) 76.
[113] I. Samaras, S.I. Saikh, C. Julien, M. Balkanski, Mater. Sci. Eng. B 3 (1989) 209.
[114] L.S. Selwyn, W.R. McKinnon, U. von Sacken, C.A. Jones, Solid State Ionics 22 (1987) 337.
[115] M.A. Santa Ana, G. González, Bol. Soc. Chil. Quím. 37 (1992) 157.
[116] C. Julien, T. Sekine, M. Balkanski, Solid State Ionics 48 (1991) 225.
[117] T. Sekine, C. Julien, I. Samaras, M. Jouanne, M. Balkanski, Mater. Sci. Eng. B 3 (1989) 153.
[118] C.A. Papageorgopoulos, W. Jaegermann, Surf. Sci. 338 (1995) 83.
[119] N. Imanishi, M. Toyoda, Y. Takeda, O. Yamamoto, Solid State Ionics 58 (1992) 333.
[120] K. Chrissafis, M. Zamabi, K. Kambas, J. Stoemeros, N.A. Economou, I. Samaras, C. Julien, Mater. Sci. Eng. B 3 (1989) 145.
[121] S. Jiménez Sandoval, D. Yang, R.F. Frindt, J.C. Irwin, Phys. Rev. B 44 (1991) 3955.
[122] D. Yang, S. Jiménez Sandoval, W.M.R. Divigalpitiya, J.C. Irwin, R.F. Frint, Phys. Rev. B 43 (1991) 12043.
[123] P. Joensen, E.D. Crozier, N. Alberding, R.F. Frint, J. Phys. C: Solid State Phys. 20 (1987) 4043.
[124] J. Heising, M.G. Kanatzidis, J. Am. Chem. Soc. 121 (1999) 638.
[125] B.E. Brown, Acta Crystallogr. 20 (1966) 268.
[126] H.L. Tsai, J. Heising, J.L. Schindler, C.R. Kannewurf, M.G. Kanatzidis, Chem. Mater. 9 (1997) 879.
[127] F. Wypych, K. Sollmann, R. Schöllhorn, Mater. Res. Bull. 27 (1992) 545.
[128] F. Wypych, Th. Weber, R. Prins, Chem. Mater. 10 (1998) 723.
[129] K.A. Yee, T. Hughbanks, Inorg. Chem. 30 (1991) 2321.
[130] L.F. Mattheiss, Phys. Rev. B 8 (1973) 3719 (and references therein).
[131] R. Edmondson, Solid State Commun. 10 (1972) 1085.
[132] J.B. Goodenough, Phys. Rev. 171 (1968) 466.
[133] R. Huisman, R. de Jonge, C. Hass, F. Jellinet, J. Solid State Chem. 3 (1971) 56.
[134] A. Tan, S. Harris, Inorg. Chem. 37 (1998) 2205.
[135] M. Kertesz, R. Hoffman, J. Am. Chem. Soc. 106 (1984) 3453.
[136] M.-H. Whangbo, E. Canadell, J. Am. Chem. Soc. 114 (1992) 9587 (and references therein).
[137] J.K. Burdett, T. Hughbanks, Inorg. Chem. 24 (1985) 1741.
[138] C. Rovira, M.-H. Whangbo, Inorg. Chem. 32 (1993) 4094.
[139] J.C. Wildervanck, F.J. Jellineck, J. Less-Common Met. 24 (1971) 73.
[140] N.W. Alcock, A. Kjekshus, Acta Chem. Scand. 19 (1965) 79.
[141] W.Y. Liang, in: M.S. Dresselhaus (Ed.), Intercalation in Layered Materials. In: Nato ASI Series B, vol. 148, Plenum Press, New York, 1990.
[142] W.Y. Liang, Mater. Sci. Eng. B 3 (1990) 139.
[143] A.J. Berlinsky, W.G. Unruh, W.R. McKinnon, R.R. Haering, Solid State Commun. 31 (1979) 135.
[144] W.R. MacKinnon, in: A.R. Legrand, S. Flandrois (Eds.), Chemical Physics of Intercalation. In: NATO ASI Series B, vol. 172, Plenum Press, New York, 1992, p. 181.
[145] B.G. Silbernagel, W.S. Wittingham, J. Chem. Phys. 64 (1976) 3670.
[146] G. González, H. Binder, Bol. Soc. Chil. Quím. 41 (1996) 121.
[147] F. Mendizábal, R. Contreras, A. Aizman, Theochemistry 335 (1995) 161.
[148] F. Mendizábal, R. Contreras, A. Aizman, J. Phys.: Condens. Matter. 9 (1997) 3011.
[149] F. Mendizábal, R. Contreras, A. Aizman, Int. J. Quantum Chem. 58 (1995) 819.
[150] F. Mendizábal, M.A. Santa Ana, E. Benavente, G. González, unpublished results.
[151] M.A. Santa Ana, E. Benavente, J. Páez, G. González, Bol. Soc. Chil. Quim. 45 (2000) 491.
[152] R. Schöllhorn, Angew. Chem. 92 (1980) 1015.
[153] W.M.R. Divigalpitiya, R.F. Frindt, S.R. Morrison, Science 246 (1989) 369.
[154] W.M.R. Divigalpitiya, R.F. Frindt, S.R. Morrison, J. Mater. Res. 6 (1991) 1103.
[155] R. Schöllhorn, A. Weiss, J. Less-Common Met. 36 (1974) 229.
[156] E. Benavente, G. González, Bol. Soc. Chil. Quím. 42 (1997) 555.
[157] P. Joensen, R.F. Frindt, R. Morrison, Mater. Res. Bull. 21 (1986) 457.
[158] W.M.R. Divigalpitiya, S.R. Morrison, R.F. Frindt, Thin Solid Films 186 (1990) 177.
[159] Y. Santiago, C.R. Cabrera, J. Electrochem. Soc. 141 (1994) 629.
[160] A.S. Golub, I.B. Shumilova, Yu.N. Novikov, J.L. Mansot, M. Danot, Solid State Ionics 91 (1996) 307.
[161] X. Zhou, D. Yang, R.F. Frindt, J. Phys. Chem. Solids 57 (1996) 1137.
[162] H. Tagaya, T. Hashimoto, M. Karasu, T. Izumi, K. Chiba, Chem. Lett. (1991) 2113.
[163] L. Wang, J. Schindler, J.A. Thomas, C.R. Kannewurt, M. Kanatzidis, Chem. Mater. 7 (1995) 1753.
[164] R. Bissessur, J.L. Schindler, C.R. Kannewurf, M. Kanatzidis, Mol. Cryst. Liq. Cryst. 245 (1994) 249.
[165] J.P. Lemmon, J. Wu, C. Oriakhi, M.M. Lerner, Electrochim. Acta 40 (1995) 2245.
[166] J.P Lemmon, M.M. Lerner, Chem. Mater. 6 (1994) 207.
[167] E. Ruiz-Hitzky, R. Jiménez, B. Casal, V. Manríquez, A. Santa Ana, G. González, Adv. Mater. 5 (1993) 738.
[168] C.O. Oriakhi, R.L. Nafshun, M.M. Lerner, Mater. Res. Bull. 31 (1996) 1513.
[169] G. González, M.A. Santa Ana, E. Benavente, J.P. Donoso, T.J. Bonagamba, N.C. Mello, H. Panepucci, Solid State Ionics 85 (1996) 225.
[170] V. Sánchez, E. Benavente, M.A. Santa Ana, G. González, Chem. Mater. 11 (1999) 2296.
[171] E. Benavente, V. Sánchez, M.A. Santa Ana, G. González, Spring Meeting MRS, San Francisco, California, USA., 24–28 April 2000.
[172] L. Kosidowski, A.V. Powell, Chem. Commun. (1998) 2201.
[173] R. Bissessur, J. Heising, W. Hirpo, M. Kanatzidis, Chem. Mater. 8 (1996) 318.
[174] J. Brenner, C. Marshall, L. Ellis, N. Tomczyk, J. Heising, R. Bissessur, M.G. Kanatzidis, Chem. Mater. 10 (1998) 1244.
[175] J. Heising, F. Bonhomme, M. Kanatzidis, J. Solid. State Chem. 139 (1998) 22.
[176] M. Danot, J.L. Mansot, A.S. Golub, G.A. Protzenko, P.B. Fabritchnyi, Yu.N. Novikov, J. Rouxel, Mater. Res. Bull. 29 (1994) 833.
[177] A.S. Golub, G.A Protzenko, I.M. Yanovskaya, O.L. Lependina, Yu.N. Novikov, Mendeleev Commun. (1993) 199.
[178] Y.V. Zubavichus, Y.L. Slovokhotov, L. Yurii, P.J. Schilling, R.C. Tittsworth, A.S. Golub, G.A. Protzenko, Y.N. Novikov, Inorg. Chim. Acta 280 (1998) 211.
[179] E.A. Gash, A.L. Spain, L.M. Dyslesky, C.J. Flaschenriem, A. Kalaveshi, P.K. Dorhout, S.H. Strauss, Environ. Sci. Technol. 32 (1998) 1007.
[180] Y.V. Zubavichus, A.S. Golub, Y.N. Novikov, Y.L. Slovokhotov, Y.L. Nesmeyanov, P.J. Schilling, R.C. Tittsworth, J. Phys. IV 7 (1977) 1057.
[181] M.B. Dines, Science 188 (1974) 1210.

[182] A.S. Golub, I.B. Shumilova, Yan Y. Zubavichus, M. Jahncke, G. Süss-Fink, M. Danot, Yu.N. Novikov, J. Mater. Chem. 7 (1997) 163.
[183] G. González, M.A. Santa Ana, E. Benavente, Electrochim. Acta 43 (1998) 1327.
[184] S. Basu, W.L. Worrel, in: P. Vashista, J.N. Mundy, G.K. Sheny (Eds.), Fast Ion Transport in Solids, North-Holland, Amsterdam, 1979.
[185] G. González, M.A.Santa Ana, E. Benavente, J. Phys. Chem. Solids 58 (1997) 1457.